Does evolution design robust food webs?

Pavanee Annasawmy, Jean-François Ternon, Pascal Cotel, Yves Cherel, Evgeny Romanov, Gildas Roudaut, Anne Lebourges-Dhaussy, Frédéric Ménard, Francis Marsac

Micronekton distributions and assemblages at two shallow seamounts of the south-western Indian Ocean: Insights from acoustics and mesopelagic trawl data

Pavanee Annasawmy[1, 2*], Jean-François Ternon[1], Pascal Cotel[1], Yves Cherel[3], Evgeny V. Romanov[4], Gildas Roudaut[5], Anne Lebourges-Dhaussy[5], Fréderic Ménard[6], Francis Marsac[1, 2]

[1] *MARBEC, Univ Montpellier, CNRS, Ifremer, IRD, Avenue Jean Monnet, CS 30171, 34203 Sète cedex, France*

[2] *Department of Biological Sciences and Marine Research Institute, University of Cape Town, Private Bag X3, Rondebosch 7701, Cape Town, South Africa*

[3] *Centre d'Etudes Biologiques de Chizé (CEBC), UMR7372 du CNRS-Université de la Rochelle, 79360 Villiers-en-bois, France*

[4] *Centre technique d'appui à la pêche réunionnaise (CAP RUN)-NEXA, 97420 Le Port, Île de la Réunion, France*

[5] *Institut de Recherche pour le Développement (IRD), UMR LEMAR 195 (UBO/CNRS/IRD), Campus Ifremer, BP 70, 29280 Plouzané, France*

[6] *Aix Marseille Univ, Université de Toulon, CNRS, IRD, MIO, Marseille, France*

* Corresponding author: angelee-pavanee.annasawmy@ird.fr

Abstract

Micronekton distributions and assemblages were investigated at two shallow seamounts of the south-western Indian Ocean using a combination of trawl data and multi-frequency acoustic visualisation techniques. La Pérouse (~60 m) seamount is located on the outskirts of the oligotrophic Indian South Subtropical Gyre province with weak mesoscale activities and low primary productivity all year round. The "MAD-Ridge" seamount (thus termed in this study; ~240 m) is located in the productive East African Coastal (EAFR) province with high mesoscale activities to the south of Madagascar. This resulted in higher micronekton species richness at MAD-Ridge compared to La Pérouse. Resulting productivity at MAD-Ridge seamount was likely due to the action of mesoscale eddies advecting larvae and productivity from the Madagascar shelf rather than local dynamic processes such as Taylor column formation. Mean micronekton abundance/biomass, as estimated from mesopelagic trawl catches, were lower over the summit compared to the vicinity of the seamounts, due to net selectivity and catchability and depth gradient on micronekton assemblages. Mean acoustic densities in the night shallow scattering layer (SSL: 10-200 m) over the summit were not significantly different compared to the vicinity (within 14 nautical miles) of MAD-Ridge. At La Pérouse and MAD-Ridge, the night and day SSL were dominated by common diel vertical migrant and non-migrant micronekton species respectively. While seamount-associated mesopelagic fishes such as *Diaphus suborbitalis* (La Pérouse and MAD-Ridge) and *Benthosema fibulatum* performed diel vertical migrations (DVM) along the seamounts' flanks, seamount-resident benthopelagic fishes, including *Cookeolus japonicus* (MAD-Ridge), were aggregated over MAD-Ridge summit both during the day and night. Before sunrise, mid-water migrants initiated the first vertical migration event from the intermediate to the deep scattering layer (DSL, La Pérouse: 500-650m; MAD-Ridge: 400-700 m) or deeper. During sunrise, the other taxa contributing to the night SSL exhibited a successive series of vertical migration events from the surface to the DSL or deeper. Some scatterers were blocked in their upward and downward migrations due to the seamount topography, more commonly known as the sound scattering layer interception/topographic blockage hypothesis. Possible mechanisms leading to the observed patterns in micronekton vertical and horizontal distributions are discussed. This study contributes to a better understanding of how seamounts influence the diel vertical migration, horizontal distribution and community composition of micronekton and seamount-associated/resident species at two poorly studied shallow topographic features in the south-western Indian Ocean.

34 Keywords: micronekton, seamount, south-western Indian Ocean, acoustics, seamount-
35 associated fauna

36

1. Introduction

Seamounts are ubiquitous underwater topographic features, usually of volcanic origin, which rise steeply through the water column from abyssal depths. They exhibit various shapes (conical, circular, elliptical or elongated) with the summit reaching various depths below the sea surface. Shallow seamounts are those reaching into the euphotic zone. As topographic obstacles, seamounts may influence prevailing ocean currents by disrupting the oceanic flow and causing spatial and temporal variability in the current field (Royer, 1978; White et al., 2007). The combined interaction of various seamount characteristics, stratification and oceanic flow conditions may provide local dynamic responses at seamounts such as formation of a Taylor Column or Cone, isopycnal doming (Mohn & Beckmann, 2002), enclosed circulation cells and enhanced vertical mixing (White et al., 2007). The aforementioned physical processes may cause various responses over seamounts, notably, upwelling and vertical mixing of nutrient-rich waters from deeper to shallower layers and enhanced productivity (Boehlert & Genin, 1987; Genin, 2004). The enclosed, semi-enclosed circulation pattern around seamounts may also be important retention mechanisms for drifting organisms produced over, or advected from the far field into the vicinity of the seamount (White et al., 2007).

Seamounts are important for fisheries around the world since they aggregate large pelagic organisms of commercial value such as tunas (Fonteneau, 1991; Holland & Grubbs, 2007; Dubroca et al., 2013), alfonsinos and orange roughy (Ingole & Koslow, 2005; Bensch et al., 2009). In the southwestern Indian Ocean seamount-associated fisheries gradually developed since the early 1970s, targeting various species, including alfonsinos (*Beryx* sp.), rubyfish (*Plagiogeneion rubiginosus*), cardinalfish (*Epigonus* sp.), pelagic armourhead (*Pentaceros richardsoni*), rudderfish (*Centrolophus niger*), bluenose (*Hyperoglyphe antarctica*), and later expanded to orange roughy (*Hoplostethus atlanticus*) and oreos (Oreosomatidae) throughout

62 ridge systems of the southern Indian Ocean including Walters Shoal and deeper areas such as
63 Madagascar and Mozambique ridges (Collette & Parin, 1991; Romanov, 2003; Clark et al.,
64 2007; Parin et al., 2008; Rogers et al., 2017), Tunas are also subjected to fishing pressures at
65 the Travin Bank, also known as the "Coco de Mer" (Indian Ocean), since its discovery in the
66 late 1970s (Marsac et al., 2014). Several hypotheses have been proposed to explain the high
67 densities of marine megafauna associated with seamounts. La Pérouse seamount may present
68 favourable breeding habitats for humpback whales (Dulau et al., 2017). Seamounts may
69 provide navigation aids in fish movements and tunas may gather around these features to
70 enhance the encounter rate with other con-specifics (Fréon & Dagorn, 2000) or they may be
71 attracted by aggregations of prey (Holland & Grubbs, 2007; Morato et al., 2008). Organisms
72 inhabiting the mesopelagic zone, the micronekton, represent an important forage fauna for
73 top predators (Guinet et al., 1996; Cherel et al., 2010; Danckwerts et al., 2014; Jaquemet et
74 al., 2014; Potier et al., 2004, 2007, 2014).

75 Micronekton can be divided into the broad taxonomic groups- crustaceans, cephalopods,
76 fishes (Brodeur & Yamamura, 2005; De Forest & Drazen, 2009) and gelatinous organisms
77 (Lehodey et al., 2010; Kloser et al., 2016). They typically range in size from 2-20 cm. They
78 form dense sound-scattering layers since some of them reflect sound in the water, due to their
79 swimbladders, hard shells and gas inclusions (Simmonds & MacLennan, 2005; Kloser et al.,
80 2009). Different scatterers are expected to have different relative frequency responses
81 (Benoit-Bird & Lawson, 2016). While organisms with gas-filled structures such as epi-
82 mesopelagic fishes with gas-filled swimbladders and gelatinous organisms with
83 pneumatophores dominate the 38 kHz frequency (Porteiro & Sutton, 2007; Kloser et al.,
84 2002, 2009; 2016; Davison et al., 2015; Cascão et al., 2017; Proud et al., 2018), large
85 crustaceans, small copepods, squids and non-gas bearing fishes are relatively weak scatterers
86 at this frequency (Cascão et al., 2017; Proud et al., 2018). Euphausiid shrimps are better

87 targets at 70 kHz (Furusawa et al., 1994; Simmonds & MacLennan, 2005). Smaller plankton
88 are stronger targets at 120 kHz compared to the 38 kHz and is a commonly used feature for
89 separating plankton and fish marks on echograms (Simmonds & MacLennan, 2005).

90 Some micronekton taxa undergo diel vertical migration (DVM) from deep to shallow layers
91 (upper 200 m) at dusk and from shallow to deep layers (below 400 m) at dawn (Lebourges-
92 Dhaussy et al., 2000; Béhagle et al., 2014; Annasawmy et al., 2018). Other taxa were shown
93 to exhibit delayed migration (Watanabe et al., 2002), reverse migration (Alverson, 1961;
94 Gjosaeter, 1978, 1984; Marchal & Lebourges-Dhaussy, 1996; Lebourges-Dhaussy, 2000;
95 Annasawmy et al., 2019c), mid-water migration or non-migration (Annasawmy et al., 2018).
96 It is thought that the spatial/horizontal distribution of micronekton communities is also not
97 uniform across the Atlantic (Judkins & Haedrich, 2018) and south-western Indian Ocean
98 (Annasawmy et al., 2018). Various physical processes such as mesoscale eddies, proximity to
99 continental shelves and landmasses, and seamounts may influence micronekton's
100 distributions (Annasawmy et al., 2019c). Seamounts, by introducing irregularities into the
101 pelagic environment, such as a hard substrate, disrupted current flows, increased primary
102 productivity, entrapment of plankton, and presence of benthic predators, are thought to
103 influence the abundance, biomass, diversity and taxonomic composition of micronekton
104 (Genin 2004; Wilson & Boehlert, 2004; De Forest & Drazen, 2009).

105 Although seamounts in other ocean basins are hypothesized to have a general influence on
106 mesopelagic communities (De Forest & Drazen, 2009; Tracey et al., 2012), little is known
107 about the micronekton dynamics at La Pérouse and MAD-Ridge seamounts, two shallow
108 topographic features of the south-western Indian Ocean. La Pérouse is located 90 nautical
109 miles (nmi) to the North West of Reunion Island (Fig. 1a; Fig. 2), on the outskirts of the
110 oligotrophic Indian South Subtropical Gyre Province (ISSG) (Longhurst, 2007). The summit
111 depth is ~ 60m below the sea surface and is 10 km long with narrow and steep flanks. MAD-

112 Ridge seamount (thus termed in this study) is located along the Madagascar Ridge, 130 nmi
113 to the South of Madagascar (Fig. 1b; Fig. 2). The summit depth is 240 m below the surface
114 and is 33 km long (North to South) and 22 km wide (East to West). MAD-Ridge is located
115 within an "eddy-corridor" along the Fort Dauphin upwelling area and is frequently crossed by
116 mesoscale eddies spinning off the South East Madagascar Current (Pollard & Read, 2015;
117 Vianello et al., 2019). These eddies may become trapped over the seamount and have an
118 influence on the assemblages and DVM patterns of micronekton communities (Annasawmy
119 et al., 2019c).

120 The main objectives of this study are to investigate (1) the prevailing environmental
121 conditions at La Pérouse and MAD-Ridge seamounts using satellite data, (3) the vertical and
122 horizontal distributions of the scattering layers at MAD-Ridge using acoustic data, (2) the
123 micronekton assemblages at La Pérouse and MAD-Ridge using trawl data, and (4) whether
124 La Pérouse and MAD-Ridge summits aggregate higher biomasses/densities of micronekton
125 compared to the immediate vicinity of the seamounts, using acoustic and trawl data.

126 **2. Methods**

127 2.1 Study area and scientific cruises

128 La Pérouse cruise (DOI: 10.17600/16004500) was carried at latitude 19°43'S and longitude
129 54°10'E on board the R.V. *ANTEA* from the 15th to the 30th of September 2016, departing
130 from/returning to Reunion Island (Fig. 1a). MAD-Ridge cruise (DOI: 10.17600/16004800
131 and 10.17600/16004900) was divided into two legs: leg 1 from Reunion Island to Fort
132 Dauphin (Madagascar) from the 8th to the 24th of November 2016, and leg 2 from Fort
133 Dauphin (Madagascar) to Durban (South Africa) from the 26th of November to the 14th of
134 December 2016. MAD-Ridge seamount (latitude 27°28.38'S and longitude 46°15.67'E), was

sampled for acoustics and trawling during leg 2 of this cruise on board the R.V. *ANTEA* (Fig. 1b).

2.2 Satellite monitoring of La Pérouse and MAD-Ridge seamounts

Delayed-time mean sea level anomalies (MSLAs) at a daily and 1/4° resolution, produced and distributed by the Copernicus Marine Environment Monitoring Service project (CMEMS) and available at http://marine.copernicus.eu/, were used to describe the mesoscale eddy field at the time of La Pérouse and MAD-Ridge cruises. Sea surface chlorophyll (SSC) data, with a daily and 4.5 km resolution was downloaded from the MODIS sensor (http://oceancolor.gsfc.nasa.gov) and was used to calculate 5-day averages to obtain a proxy of surface oceanic primary production. Monthly mean chlorophyll *a* concentrations for the defined regions (La Pérouse: 18.5°-20°S/53°-55°E; MAD-Ridge: 27°-28°S/44°-48°E; Fig. 2c) were averaged from January to December 2016 to investigate the annual variability in chlorophyll *a* concentration/productivity.

2.3 Acoustic surveys

Acoustic surveys were carried out with a Simrad EK60 echosounder operating at four frequencies during both cruises: 38 kHz (750 m of acquired range), 70 kHz (500 m), 120 kHz (250 m) and 200 kHz (150 m). The transducers were calibrated prior to the cruises following the procedures recommended in Foote et al. (1987). The pulse duration was set at 0.512 ms and the transmitted power at 1000 W (38 kHz), 750 W (70 kHz), 200 W (120 kHz) and 90 W (200 kHz) during data acquisition periods. The water column was correctly sampled to a depth of 750 m during data acquisition for the 38 kHz frequency. La Pérouse acoustic data were intermittently recorded during transits and few mesopelagic trawl stations. The acoustic transects during MAD-Ridge transit periods were petal-shaped (Petals I-VII, see Fig. 3a), starting from the seamount summit either at sunset between 3:48pm and 4:10pm Universal

Time (Petals I-II) or at night between 6:13pm and 7:20pm Universal Time (Petals III-VII) till the next morning between 05:38am and 06:29am (see Fig. 3b-h).

Acoustic data were processed with the Matecho software (an open source IRD tool computed with MATLAB 7.11.0.184, Release 2010b- and based on the Ifremer's Movies3D software; Trenkel et al., 2009; Perrot et al., 2018). Acoustic data sampled during transit (~ 8-9 knots) and trawl stations (~ 2-3 knots) were processed and echo-integrated separately, with different parameters to account for the differing ship speed. Transient (multiple pings) and background noises, bottom echoes and attenuated signals were removed using the algorithms designed by De Robertis & Higginbottom (2007) and Ryan et al. (2015). The first 10 m below the sea surface was removed to account for the presence and over amplification of the signal due to surface bubbles. Echo-integrations of acoustic data were performed on 1-m layers at a threshold of -80 dB to exclude scatterers not representative of the micronekton community (Béhagle et al., 2017). The echo-integration cell size was fixed at 0.1 nmi during transit periods and at 10 pings during trawl stations. The volume backscattering strength (S_V, dB re 1 m^{-1}, MacLennan et al., 2002) was calculated to obtain the relative acoustic densities of scatterers per unit volume. The water column was separated into three depth categories, based on epi-mesopelagic layers: surface/shallow (10-200 m), intermediate (200-400 m) and deep (400-750 m).

Red Green Blue (RGB) composite images were generated in MATLAB (version 2016), based on the 38, 70 and 120 kHz MAD-Ridge echo-integrated acoustic data. This acoustic visualisation technique is useful in determining the relative contribution of each frequency to the overall backscatter, in identifying the different scattering layers and identifying dense micronekton aggregations. It is used to enhance and colour-code sample volumes with similar acoustic features. The 38, 70 and 120 kHz echo-integrated acoustic data were given in red, green and blue colour codes respectively on each RGB plot, with the dynamic of the S_V

184 values for each frequency being converted in 256 levels of each colour. A linear
185 transformation of the backscatter was applied for each frequency:

186 Color index (0 to 255) = [255/ (High scale threshold- Low scale threshold)] x [S_V (fr) – Low
187 scale threshold], whereby

188 the high scale threshold is the maximum backscatter for hue visualisation, the low scale
189 threshold is the minimum backscatter for hue visualisation and S_V (fr) is the backscatter value
190 at frequency (fr) which can be the 38 kHz/70 kHz/120 kHz frequency.

191 In the resulting RGB composite, the "hue" gives the frequency with the highest backscatter.
192 On an RGB composite image based on the 38, 70 and 120 kHz echo-integrated acoustic data
193 and given in red, green and blue color codes respectively, a dark red colour indicates a
194 dominant but low 38 kHz backscatter, whereas a light red colour indicates a dominant and
195 high 38 kHz backscatter. The same rule applies to the blue (70 kHz) and green (120 kHz)
196 hues. A black dominating hue on the RGB plot indicates that all backscatters are under the
197 low scale threshold of -80 dB whereas a white dominating colour indicates that all
198 backscatters are close to the high scale threshold of -50 dB.

199 2.4 Net sampling

200 Ten epi-mesopelagic tows were performed at La Pérouse and 17 tows at MAD-Ridge (Table
201 1; Fig. 1a and 1b). Trawl MZC was carried in the Mozambique Channel (Fig. 1) and will be
202 used as reference for open-water trawls compared to trawls 1-17 carried at MAD-Ridge
203 seamount. A 40m long International Young Gadoid Pelagic Trawl (IYGPT) was used, having
204 an 80 mm knotless nylon delta mesh netting at the front tapering and 5 mm at the codend and
205 a mouth opening of ~ 96 m^2. The trawl was towed at a ship speed of 2-3 knots at the targeted
206 depth for 60 minutes during La Pérouse cruise and 30 minutes during MAD-Ridge cruise.
207 During both cruises, the sampling depth was that of the sound scattering layer in that ship

position and at that time of day, with no rigid plan of sampling preselected depths. Trawl depth was monitored with a Scanmar depth sensor during both cruises. The total volume of water filtered by the net tows was calculated by multiplying the distance travelled during the tows by the area of the trawl mouth opening to account for the differing sampling durations during the cruises. The total volume of water filtered during La Pérouse ranged from 379 408 m^3 to 871 181 m^3, and from 154 086 m^3 to 312 321 m^3 during MAD-Ridge. Trawl stations were further classified into the categories summit, flank and vicinity according to whether they occurred on the summit plateaus of the seamounts, on the slopes or in the vicinity of the seamounts (i.e. any trawl not carried out on the summit and flanks) (Table 1.0).

The micronekton organisms collected during both cruises were sorted on board, divided into four broad categories: gelatinous organisms, crustaceans, cephalopods and fishes. The wet mass (WM) in grams was recorded for each category. Total length of selected gelatinous organisms, abdomen and carapace length of selected crustaceans, dorsal mantle length of selected cephalopods and standard length of fishes were measured. The micronekton components were counted and identified to the lowest possible taxon on board and also onshore from frozen samples preserved at -20°C. The total micronekton abundance estimates were calculated by dividing the total number of individuals per trawl by the volume of water filtered and multiplying by the average thickness of the day/night backscattering layer (100 m) and expressed as abundance within the backscattering layer (ind. m^{-2}) (as in Kwong et al., 2018). Similarly, the total biomass of organisms collected per trawl (g WM m^{-2}) was calculated by dividing the total wet mass (WM g) of micronekton broad categories per trawl by the volume of water filtered and multiplying by the average thickness of the day/night backscattering layer (100 m). The habitat ranges of available micronekton taxa were obtained from literature (Clarke & Lu, 1975; Pearcy et al., 1977; Smith & Heemstra, 1986; Van der Spoel & Bleeker, 1991; Brodeur & Yamamura, 2005; Davison et al., 2015; Romero-Romero

et al., 2019). Detailed fish species size distributions and compositions from both La Pérouse and MAD-Ridge cruises are described in Cherel et al. (2019). Detailed habitat and size ranges, and trophic positions of selected micronekton taxa are given in Annasawmy et al. (2019a).

2.5 Data visualization and statistical analyses

La Pérouse and MAD-Ridge seamount bathymetry data were acquired with the 12 kHz frequency of a Simrad EA 500 echosounder and the 38 kHz of the Simrad EK60 echosounder. The bathymetry data were interpolated on a regular grid using the software Surfer Version 10.3.705. Wilcoxon rank sum tests were performed to investigate the differences in mesopelagic trawl abundance and biomass estimates between La Pérouse and MAD-Ridge and the mean acoustic densities over the summit and vicinity of MAD-Ridge.

Micronekton species richness was calculated using R (3.3.1) vegan package (2.5-1, Oksanen et al., 2018). The PRIMER v6 software was used to perform multivariate analyses according to Clarke & Warwick (2001) on La Pérouse and MAD-Ridge micronekton abundance datasets to test for the effects of depth, trawl location and time of day on micronekton abundance and to identify the shallow-dwelling/deep-dwelling and seamount-associated/resident fauna. The fourth root transformation was used on species abundance data to down-weight strongly abundant species, thus allowing rare species to exert some influence on the similarity calculation (Clarke & Warwick, 2001). Resemblance matrices were created from the Bray-Curtis measure of similarity and were used to run the SIMPROF (similarity profile) permutation testing to identify statistically significant cluster of samples. Non-metric dimensional scaling (MDS) were used to produce 2-dimensional ordination of samples according to the selected grouping variables Depth category, Trawl location and Time of day. Bubble plots were overlaid on the MDS ordination diagrams to represent the relative

abundance of the selected species per trawl station (plotted at the bubble centres). The larger the bubble, the greater the mean number of individuals were captured at that site. One-way ANOSIM (analysis of similarities) was calculated to test for significant differences in the micronekton community composition according to the factors Depth, Trawl location and Time of Day. The SIMPER (similarity percentages) analysis was carried out to identify the taxa contributing most to the similarities/dissimilarities within each resultant cluster group.

3. Results

3.1 Prevailing environmental conditions at La Pérouse and MAD-Ridge seamounts

During La Pérouse cruise in September 2016, the seamount was under the influence of a weak cyclonic eddy with a MSLA of ~ -10 cm (Fig. 2a). MAD-Ridge was under the influence of an eddy dipole with the anticyclonic feature being trapped on the seamount during the cruise in November 2016 (Fig. 2b). The MSLA at MAD-Ridge was ~10 cm (eddy periphery) to 40 cm (core of the anticyclone) during leg 1 of the cruise. The annual primary productivity, derived from satellite observations, followed the same pattern in both regions of La Pérouse and MAD-Ridge seamounts, with maximum values reached in July, as a result of an intense mixing caused by the austral winter trade winds, and minimum values observed during austral summer (January-March and November-December) (Fig. 2c). Both La Pérouse and MAD-Ridge cruises took place during a decreasing trend of oceanic productivity. Although, the annual mean chlorophyll *a* concentration depicted the same cycle at both seamounts, chlorophyll *a* concentrations at MAD-Ridge were twice higher than at La Pérouse all year round.

3.2 Vertical and horizontal distributions of biological scatterers at MAD-Ridge

The highest mean acoustic densities (S_V) of the 38 kHz frequency were observed at night in the surface layer (10-200 m) across all petals (I-VII) at MAD-Ridge (Fig. 3a-h). The mean

281 acoustic densities in the surface layer showed a decreasing trend at sunrise and during day
282 time (Petals I to VII, Fig. 3b-h) while gradually increasing in the deep layer across petals II to
283 VI (Fig. 3c-g). The intermediate layer showed the lowest acoustic densities compared to the
284 surface and deep layers, although a peak can be observed during sunrise when organisms
285 vertically migrated towards deeper layers. A peak in day time acoustic densities in the deep
286 layer can be observed across petals II and IV (Fig. 3c and 3e) over the seamount flanks,
287 which can be attributed to topographic blockage of biological scatterers (Fig. 4a, b and c).

288 Echograms of the 38 kHz frequency showed organisms migrating from below 400 m (deep)
289 to above 200 m (surface) at dusk across Petal II (Fig. 4a). Biological scatterers were also
290 shown to perform a successive series of DVM events from the intermediate/surface layers to
291 deeper layers before sunrise and during sunrise, reaching the DSL before day time (Fig. 4a, b
292 and c). Across petals IV, an increase in the mean acoustic densities in the day time DSL can
293 be observed (Fig. 3e), indicating a likely downward migratory trend of the biological
294 scatterers to deeper layers and blockage and/or preferential association of some micronekton
295 taxa with the flanks of MAD-Ridge seamount (Fig. 4c). A dense SSL between ~10-200 m
296 and a DSL between ~400-700 m were observed throughout the night during MAD-Ridge
297 cruise (Fig. 4a, b and c). After vertical migration of scatterers to deeper depths at dawn, the
298 day SSL became less dense (compared to the night SSL) and persisted in the top 100 m of the
299 water column. Biological scatterers were associated with MAD-Ridge seamount summit and
300 flanks both during night time and day time.

301 To investigate the influence of MAD-Ridge summit, the mean night time acoustic densities of
302 the 38 kHz frequency between 10-250 m over the summit and at the seamount vicinity
303 (within 14 nmi from the summit) were investigated along petals III-VII (Fig. 5a, b and c).
304 Petals I and II were discarded since these transects were incomplete, not being carried from
305 the summit. The mean acoustic densities between the summit and vicinity of MAD-Ridge

seamount were not statistically different (W=43610, $p > 0.05$). The highest acoustic responses to the 38 kHz frequency in the surface layer (10-250 m) at night can be observed across Petals IV and V, while Petal VI exhibited the lowest acoustic responses (Fig. 5b). RGB composites of the 38, 70 and 120 kHz frequencies across petals III-VII showed distinct scattering layers in the top 150 m of the water column, with some scatterers being strong targets at the 38 kHz frequency and others at the 70 kHz frequency (Fig. 5c). The peak in acoustic densities at 0.1 nmi across petal IV (Fig. 5b) may be attributed to the relatively high S_V at ~250 m (i.e. below the night SSL) on the seamount summit. Patches of relatively high S_V (seen as "white patches") can be observed on the seamount summit across petals IV, V and VII (Fig. 5c).

3.3 Taxonomic composition of trawl catches

At La Pérouse seamount, 147 taxa from 10 trawls representing 7, 16, 17 and 107 taxonomic groups of gelatinous organisms, crustaceans, cephalopods and epi-mesopelagic fishes, respectively, were collected. At MAD-Ridge, 149 taxa from 17 trawls, representing 5, 13, 17 and 114 taxonomic groups of gelatinous organisms, crustaceans, cephalopods and epi-mesopelagic fishes, respectively, were collected. Six individuals of the benthopelagic fish species, *Cookeolus japonicus*, were further collected at MAD-Ridge seamount summit (Fig. 8d, 9b and 10c). MAD-Ridge and La Pérouse trawls caught 3, 12, 14 and 66 identical taxa of gelatinous organisms (jellyfish, salps and pyrosomes), crustaceans, cephalopods and epi-mesopelagic fishes respectively.

Micronekton abundance and biomass estimates were greater at MAD-Ridge compared to La Pérouse (Fig. 6a), however, values were not significantly different (Abundance:, W= 144.5, $p > 0.05$; Biomass: W=115, $p > 0.05$). Mean micronekton abundance and biomass estimates were lower over La Perouse summit (0.004 ind m^{-2} and 0.006 g WM m^{-2}) compared to the

330 vicinity (0.15 ± 0.11 ind m^{-2} and 0.26 ± 0.18 g WM m^{-2}). At MAD-Ridge, the summit also
331 recorded lower abundance and biomass estimates (0.03 ind m^{-2} and 0.11 g WM m^{-2})
332 compared to the vicinity (0.33 ± 0.43 ind m^{-2} and 0.46 ± 0.22 g WM m^{-2}). The species
333 richness was higher at MAD-Ridge (maximum species richness of 155) compared to La
334 Pérouse (138), with the probability of encountering new or rare species with increasing
335 fishing effort being higher at MAD-Ridge (Fig. 6b). The length distributions of organisms
336 captured during both La Pérouse and MAD-Ridge were heavily skewed towards smaller
337 sizes. Most of the micronekton captured were less than 100 mm (Fig. 6c), except for a few
338 larger nektonic squid and fish species such as Cranchiidae sp. (339 mm- mantle length) and
339 Nemichthyidae (614mm- standard length) during La Pérouse and the gelatinous *Salpa* sp.
340 (207 mm- total length), squid *Ommastrephes bartramii* (490 mm- mantle length) and fish
341 Nemichthyidae (446 mm) during MAD-Ridge.

342 Multivariate analysis of the taxa collected at La Pérouse seamount indicated that the sampling
343 depth and trawl location were significant factors influencing micronekton community
344 composition (ANOSIM, sampling depth: $R= 0.38$, $p < 0.05$; trawl location: $R= 0.52$, $p <$
345 0.05), while there was no significant effect of the time of day probably due to the low
346 daytime fishing effort (ANOSIM, $R= 0.846$, $p > 0.05$). The assemblages from the deepest
347 (400-600 m) and shallowest (0-110m) depth categories (SIMPER, average dissimilarity=
348 69.1%) and those from the vicinity and seamount summit (SIMPER, average dissimilarity=
349 81.0%) were the most dissimilar, while those from the intermediate and deep categories were
350 the least dissimilar (SIMPER, average dissimilarity= 58.3%). A main cluster at 40%
351 similarity helped differentiate the night shallow, intermediate and deep tows carried at the
352 flank and vicinity from the day trawl carried at the summit of La Pérouse (Fig. 7a).

353 The day shallow trawl over La Pérouse summit sampled a greater percentage abundance and
354 biomass of gelatinous organisms, crustaceans and fishes (Fig. 7b). Cephalopods were caught

355 most abundantly and in greater biomass during the night shallow trawls compared to the night
356 deep, intermediate and day shallow trawls (Fig. 7b and 9a). Crustaceans were caught in all
357 trawls at La Pérouse seamount (Fig. 7b) except the meso-bathypelagic crustacean *Pasiphaea*
358 sp. and *Neognathophausia* which were caught in night deep and intermediate trawls only at
359 the vicinity of the seamount as shown by bubble plot overlays of the MDS ordination (Fig.
360 7c). The sternoptychid *Argyropelecus aculeatus* and *Argyropelecus hemigymnus* were absent
361 from the shallow trawls and were caught either in the intermediate and/or deep trawls at La
362 Pérouse flanks and vicinity (Fig. 7c and 9a). The myctophid fish *Diaphus suborbitalis* was
363 caught in high numbers, both in shallow and deep layers, on the flanks of La Pérouse
364 seamount at night. La Pérouse flanks also hosted four individuals of the sternoptychid
365 *Argyripnus hulleyi* in the deep layer at night (Fig. 7d and 9a).

366 At MAD-Ridge, sampling depth, time of day and trawl location were significant factors
367 influencing the micronekton community composition as shown by multivariate analyses of
368 the micronekton taxa and species abundance data (Effect of sampling depth: ANOSIM, R=
369 0.351, $p < 0.05$; Effect of time of day: ANOSIM, R=0.369, $p < 0.05$; Effect of trawl location:
370 ANOSIM, R=0.205, $p < 0.05$). A main cluster at 35% similarity confirmed a depth gradient
371 in community composition in shallow and deep layers (Fig. 8a). Clusters at 30% similarity
372 helped differentiate samples collected during night shallow tows at the seamount summit and
373 flanks from all other tows carried out during the cruise. The micronekton assemblages from
374 the deepest (440-550 m) and shallowest (0-210m) depth categories were the most dissimilar
375 (SIMPER, average dissimilarity= 69.9%; ANOSIM, R= 0.477, $p < 0.05$) and those from the
376 intermediate and deep categories were the least dissimilar (SIMPER, average dissimilarity=
377 50.8%; ANOSIM, R=-0.333, $R > 0.05$).

378 The majority of crustacean species were caught across all trawls (Fig. 8b), except *Pasiphaea*
379 sp. caught in night deep trawls only (Fig. 9b). Cephalopods were caught most abundantly and

380 in greater biomasses in the shallow trawls compared to the intermediate and deep trawls (Fig.
381 8b and 9b). Gelatinous organisms and fishes were abundantly caught across all trawls in the
382 shallow, intermediate and deep layers and at MAD-Ridge seamount summit, flanks and
383 vicinity (Fig. 8b). Juveniles of the reef-associated epipelagic fish Acanthuridae sp. was
384 abundantly caught in night shallow trawls at the vicinity of MAD-Ridge seamount and not in
385 the deep trawls (Fig. 8c and 9b). The vertical migrant *Ceratoscopelus warmingii*
386 (Myctophidae) was abundantly caught in the shallow, intermediate and deep layers at the
387 flanks and seamount vicinity (Fig. 8c and 9b). The fish *Cyclothone* sp. (Gonostomatidae) and
388 *A. aculeatus* (Sternoptychidae) were absent from the shallow trawls during MAD-Ridge
389 cruise (Fig. 8d and 9b). MAD-Ridge seamount attracted the mesopelagic fishes *D.*
390 *suborbitalis*, *Benthosema fibulatum*, *Diaphus knappi* and *Neoscopelus macrolepidotus* (Fig.
391 8e). The summit also consisted of the apparently settled population of the benthopelagic *C.*
392 *japonicus* as shown by bubble plot overlays of the MDS ordination (Fig. 8e).

393 3.4 Micronekton community compositions and acoustic backscatter intensities

394 At La Pérouse seamount, the gelatinous plankton *Pyrosoma* sp. and salps, the crustacean
395 Natantia sp., phyllosoma larvae, the squid *Abraliopsis* sp., leptocephali larvae and the fish *C.*
396 *warmingii* were caught across almost all trawls in the night SSL and DSL over the flanks and
397 vicinity of the seamount (Fig. 9a). At MAD-Ridge seamount, *Pyrosoma* sp., salps,
398 phyllosoma larvae, *Abraliopsis* sp. and the squid Enoploteuthidae sp. were caught across
399 almost all trawls in the day and night SSL, DSL and intermediate layer over the summit,
400 flanks and vicinity of the seamount (Fig. 9b). The myctophid fish *Hygophum hygomii* was
401 abundantly caught over the summit, flanks and in the vicinity of MAD-Ridge (Fig. 9b). Since
402 the IYGPT net had no closing device, shallow water species might have contributed to the
403 catch in deeper trawls as the net was lowered and retrieved.

The backscatter intensity within the day SSL between 10-100 m over La Pérouse summit was lower compared to MAD-Ridge summit (Fig. 9a and b). Over La Pérouse summit, the day SSL consisted of a greater percentage abundance and biomass of gelatinous organisms including various types of jellyfishes, salps, and the siphonophore Diphyidae along with three leptocephali larvae and one juvenile of *Chaetodon* sp. (9a). The night SSL during La Pérouse cruise extended from the surface to 200 m. Over La Pérouse flanks, the night SSL consisted of high numbers of the crustacean Natantia sp. and the meso-bathypelagic squid *Abraliopsis* sp. and lower numbers of the cephalopods Cranchiidae sp., Oegopsida sp., *Abralia* sp., and Octopoda sp., and epi-, meso- and bathypelagic fishes of the Gonostomatidae, Malacosteidae, Myctophidae, Paralepididae and Synodontidae families. The night SSL in the vicinity of La Pérouse included similar specimens as those sampled over the flanks, such as *Pyrosoma* sp., jellyfishes, salps, Natantia sp., phyllosoma larvae, *Abraliopsis* sp., Cranchiidae sp., and Octopoda sp., and various types of fishes of the Myctophidae family.

The DSL over the flanks and vicinity of La Pérouse was less dense at night time compared to day time and was located between 500-650 m compared to MAD-Ridge (400-700 m) (Fig. 9a). The night deep trawls over La Pérouse flanks consisted of the seamount-associated fish *D. suborbitalis* in high numbers, the deep-dwelling *A. aculeatus*, the fish *A. hulleyi* (also see Cherel et al., 2019), and a variety of crustaceans and gelatinous plankton in lower numbers (Fig. 9a). *D. suborbitalis* were caught within the night SSL over the flanks of La Pérouse but not in the vicinity of the seamount. The night deep tows in the vicinity of La Pérouse consisted of the crustaceans Oplophoridae sp., Natantia sp., Sergestidae sp., Caridea sp., *Phronima* sp., *Funchalia* sp., *Pasiphaea* sp., and *Neognathophausia* sp., the cephalopods *Abraliopsis* sp. and Octopoda sp., the non-migrating fishes *A. aculeatus* and *A. hemigymnus* and diel vertically migrating and mid-water migrating fishes of the Gonostomatidae, Melanostomiidae, Myctophidae, Stomiidae, Paralepididae, Scorpaenidae and Phosichthyidae

families. Mid-water migrants showed earlier vertical migration from the intermediate to deeper layers at the end of the night, as shown by the echogram of the 38 kHz frequency. The majority of micronekton organisms however, migrated from the SSL to the DSL or deeper during sunrise in a successive series of migration events and contributed to the intensification of the backscatter within the DSL during day time. Micronekton taxa may be blocked by La Pérouse seamount in their upward migration as shown by the echogram of the 38 kHz frequency.

The night SSL over MAD-Ridge summit consisted of the gelatinous plankton salps and *Pyrosoma* sp., crustaceans Oplophoridae sp., and Natantia sp., squids Enoploteuthidae sp., *Ornithoteuthis volatilis*, *Abraliopsis* sp., and Onychoteuthidae sp., and a range of diel vertically migrating fishes of the Myctophidae, Nomeidae and Melanostomiidae families (Fig. 9b). Few individuals of the slope-associated benthopelagic fish *C. japonicus* and juveniles of the reef-associated fish *Chaetodon* sp. were collected within the night SSL over MAD-Ridge summit. The night SSL over the flanks of MAD-Ridge consisted of the crustaceans Oplophoridae sp., Sergestidae sp., *Funchalia* sp., *Euphausiacea* sp. and *Phronima* sp., squids including Ommastrephidae sp., mesopelagic fishes and high numbers of gelatinous plankton. *D. suborbitalis* were sampled in high numbers within the night SSL over the flanks and in lower numbers within the day deep tow over the flanks and in the vicinity of the seamount.

The day SSL over MAD-Ridge flanks comprised squids such as *Cranchia scabra*, *Abraliopsis* sp., Enoploteuthidae sp., and fishes such as Nemichthyidae sp., Paralepididae sp. and leptocephali. The day deep tows on the flanks and in the vicinity of MAD-Ridge consisted of a range of crustaceans and migrating fish species of the Gonostomatidae, Myctophidae, Chauliodonthidae and Photichthyidae families commonly found in deeper layers during day time. Day and night deep tows over the flanks and seamount vicinity

consisted of the non-migrating fishes *A. aculeatus*, *A. hemigymnus*, *Cyclothone* sp. Echograms of the 38 kHz frequency showed high backscatter intensities over the summit and flanks of MAD-Ridge during night time and day time due to the presence of seamount summit and flank-associated/resident species. Before sunset at MAD-Ridge vicinity, the DSL was intensified and scatterers began streaming vertically upwards. A dense night SSL was formed within the first 200 m of the water column. Some micronekton species started their vertical migration from the DSL or deeper towards the SSL before sunset, other species during sunset and at night time.

RGB composite images were analysed in conjunction with data of trawls #14, 15 and 16 to determine the acoustic responses of the micronekton captured and to make inferences about micronekton behaviour at the seamount summit as opposed to the South Mozambique Channel (trawl #21) (Fig. 10). Trawls on the seamount summit predominantly sampled dense aggregations of organisms (seen as "white patches" on RGB composites), being strong targets to the 38, 70 and 120 kHz frequencies, and having a relatively flat response to all three frequencies (Fig. 10a and c). These trawls predominantly sampled the swimbladdered myctophid fishes *D. suborbitalis* and *B. fibulatum* over MAD-Ridge flanks (Fig. 10a), the mesopelagic fishes *H. hygomii* and *N. macrolepidotus*, and the benthopelagic fish *C. japonicus* over the summit (Fig. 10c). Trawl #15 sampled a greater number of the gelatinous, *Pyrosoma* sp. which are strong targets at the 38 kHz frequency within the night SSL (Fig. 10b). Trawl #21 predominantly sampled organisms being strong targets at the 38 kHz frequency, with the fish *H. hygomii*, the squid Enoploteuthidae sp., the gelatinous *Pyrosoma* sp. and the crustaceans Oplophoridae sp. being most abundantly caught (Fig. 10d). No dense aggregations ("white patches") were observed on RGB composites of trawl #21, as opposed to trawls over the seamount summit and flanks of MAD-Ridge. Organisms were more likely

478 dispersed in the water column in the Mozambique Channel as opposed to the seamount
479 summit and flanks where they formed dense aggregations.

480

481 **4. Discussion**

482 4.1 Sampling biases and constraints

483 Pelagic trawls like the IYGPT have coarse meshes at the front through which an unknown
484 fraction of mesopelagic organisms may escape (Kaartvedt et al., 2012). Highly mobile
485 micronekton such as cephalopods and fishes may show avoidance reactions to nets which
486 may lead to discrepancies between net-based and acoustic estimates (Reid, 1991; Kaartvedt et
487 al., 2012). Organisms with fragile bodies, such as gelatinous plankton, may break apart,
488 biasing final abundance/biomass estimates (Domokos et al., 2010; Rogers et al., 2017; Proud
489 et al., 2018). La Pérouse acoustic data at sampling stations were incomplete and hence a
490 thorough comparison in mean backscatter between La Pérouse and MAD-Ridge could not be
491 carried out. Owing to bad quality acoustic data beyond 750 m, echo-integrations were limited
492 to that depth. Biases in acoustic density estimates may arise from variations in fish
493 swimbladder volume (that depends on the depth range and subsequent swimbladder
494 compression), the swimbladder size distribution and aspect (Benoit-Bird & Lawson, 2016;
495 Cascão et al., 2017; Proud et al., 2018). Some organisms also have low acoustic target
496 strengths and hence low acoustic backscatter even if found in dense aggregations on
497 seamounts (McClatchie & Combs, 2005). The RGB visualisation technique is color-vision
498 dependent but however, provides information on the mean backscatter at all three frequencies
499 on a single plot at high resolution compared to a single frequency echogram. Studies have
500 demonstrated a seasonal effect in the variability of micronekon acoustic densities (Wilson &
501 Boehlert, 2004; Cascão et al. 2017) owing to the life strategies and behaviour of the

seamount-associated fauna. This study therefore, only provided a snapshot in time of the composition of micronekton at La Pérouse and MAD-Ridge during a declining phase of oceanic productivity.

4.2 Oceanography and biological response

This study highlighted contrasting environmental patterns at La Pérouse and MAD-Ridge. While MAD-Ridge was under the influence of strong cyclonic and anticyclonic eddies originating from the South East Madagascar current, La Pérouse was under the influence of moderate mesoscale activities. As topographic obstacles, seamounts may either bifurcate, trap, split or destroy eddies (Schouten et al., 2000; Herbette et al., 2003; Adduce & Cenedese, 2004; Sutyrin, 2006; Lavelle & Mohn, 2010). Trapping duration of eddies may last several months, with important estimated effects on biological production and plankton retention (Bograd et al., 1997). Eddies are well known in influencing local water properties, such as the trapping of anomalous water masses (Swart et al., 2010; Pollard & Read, 2015), or the advection of coastal waters with high phytoplankton biomass from the coast to open waters (Quartly & Srokosz, 2004; Tew-Kai & Marsac, 2009; Kolasinski et al., 2012). Coastally upwelled waters of high biological productivity over the southern Madagascar shelf (Ramanantsoa et al., 2018) may be trapped by mesoscale features that propagate over MAD-Ridge (Annasawmy et al., 2019c).

Local productivity at MAD-Ridge did not result from a Taylor column (Annasawmy et al., 2019c) since the latter may form transiently, under specific conditions of summit depth, water column stratification and current speeds (Owens & Hogg, 1980, Freeland, 1994, Mohn et al., 2009, Wagawa et al., 2012; Bashmachnikov et al., 2013). Read & Pollard (2017) concluded that while, Taylor columns may theoretically be formed over several seamounts of the Madagascar Ridge, the relatively strong currents associated with mesoscale eddies may

prevent their formation or sweep away any incipient Taylor cap before settlement. The current speeds at La Pérouse were too high and the summit depth too shallow for Taylor column formation (Annasawmy et al., 2019c). The high yearly biological productivity at MAD-Ridge and connectivity with neighbouring seamounts of the Madagascar Ridge (Letessier et al., 2017) and with the Madagascar shelf might be one of the reasons accounting for the greater micronekton species richness and denser SSL and DSL at MAD-Ridge compared to La Pérouse. Higher mean acoustic responses were also recorded along Petal V during MAD-Ridge, which may be an aggregating effect on organisms of the strong local gradient of sea level anomalies at the anticyclonic eddy periphery (Sabarros et al., 2009).

4.3 Effect of seamounts on the DVM of micronekton

As evidenced in our study, the majority of micronekton taxa including various myctophids performed daily DVM whereas the deep-dwelling *Pasiphaea* sp., *A. aculeatus*, *A. hemigymnus* and *Cyclothone* sp. did not migrate to surface layers at dusk. Diel vertical migration did not occur as a single event, but as a successive series of events from, firstly, the mid-water migrants which migrated from the intermediate layer to the DSL or deeper before sunrise. Secondly, the surface migrants migrated from the SSL to the DSL or deeper during sunrise. Various cues such as light penetration and intensity, productivity, oxygen minima, temperature, food, clear oligotrophic waters and chemoreception of kairomones (chemical cues) released by fish, are commonly thought to influence the vertical migration of organisms and the onset of DVM (Youngbluth, 1975; Andersen et al., 1998; Cohen & Forward, 2009; Ekau et al., 2010; Bernal et al., 2015; Olivar et al., 2012, 2017). The presence of a seamount may cause some of the vertically migrating organisms to be temporarily blocked in their upward ascent/downward descent and to be concentrated on the flanks of the seamount. This "topographic blockage" mechanism/sound-scattering layer interception hypothesis has been previously described (Isaacs & Schwartzlose, 1965; Genin, 2004; Porteiro & Sutton, 2007;

Hirch & Christiansen, 2010), whereby the pre-dawn migratory descent of some mesopelagic organisms was found to be temporarily halted by the seamount topography and presence of predators using the seamount as a barrier to concentrate prey (Johnston et al., 2008).

4.4 Micronekton scattering layers and assemblages at La Pérouse and MAD-Ridge

At both La Pérouse and MAD-Ridge seamounts, the night SSL was shown to consist of gelatinous organisms (pyrosomes) and a range of common open-water swim-bladdered mesopelagic fishes that undergo DVM and are strong acoustic targets at the 38 kHz frequency. The day SSL, on the other hand, consisted of non-migrant gelatinous organisms, phyllosoma larvae, leptocephali (La Pérouse and MAD-Ridge) and few cephalopods (MAD-Ridge). While gelatinous organisms are strong targets at the 38 khz, phyllosoma larvae, leptocephali and cephalopods are relatively weak targets at this frequency. Scattering layers being strong targets at the 70 kHz frequency were observed at various distances from MAD-Ridge summit. These biological scatterers were not sampled by the IYGPT net but were shown to be associated with the depth of the maximum fluorescence (Annasawmy et al., 2019c). These organisms may be phytoplankton-eaters, siphonophores with pneumatophores smaller than those having a high response to the 38 kHz frequency (Arthur Blanluet, pers. comm.), or larger crustaceans that have a response to the 70 kHz frequency but have escaped our trawls. The day and night SSL may also have consisted of organisms that were horizontally advected in addition to species showing vertical migration (Annasawmy et al., 2019c).

A DSL was present both during the day and night at La Pérouse and MAD-Ridge seamounts. The DSL is a ubiquitous acoustic signature and is commonly formed by mesopelagic fishes and invertebrates (Aksnes et al., 2017; Proud et al., 2017). DSLs were shown to be dominated by non-migrant swimbladdered sternoptychids and gonostomatids in the Atlantic (Fennell &

575 Rose, 2015; Ariza et al., 2016), Pacific (Romero-Romero et al., 2019) and Indian Oceans,
576 south of Mauritius Island and in the Mozambique Channel (Annasawmy et al., 2018).
577 However, the DSL depth is not uniform across ocean basins. The DSL was deeper in the
578 south-western Indian Ocean at La Pérouse (500-650m), MAD-Ridge (400-700 m), south of
579 Mauritius and Reunion Islands and over the Madagascar Ridge (400-800 m) (Boersch-Supan
580 et al., 2017), compared to the Chagos Archipelago in the central Indian Ocean, where it
581 extended from 300 to 600 m (Letessier et al., 2015). Micronekton taxa showing delayed
582 vertical migration and no DVM contributed to the backscatter intensities within the night
583 DSL. Delayed vertical migration of organisms at night is commonly employed by organisms
584 to reduce competition during feeding (Watanabe et al., 2002). Some of these organisms were
585 bathypelagic species still ascending from depths deeper than 1000 m at the time that the
586 acoustic transects were conducted.

587 The most common squids sampled at La Pérouse and MAD-Ridge can be divided into the
588 following main groups (as defined by Nesis, 1993): nerito-oceanic species that occur over
589 seamounts as paralarvae, juveniles or sub-adults (eg. Onychoteuthidae and Histioteuthidae)
590 and diel vertically migrating species that are advected over seamounts at night and descend to
591 deeper depths at dawn (*Abraliopsis* sp.-Enoploteuthidae, Histioteuthidae and
592 Octopoteuthidae). *Abraliopsis* sp. may descend deeper than 1000 m during day time, hence
593 the low numbers caught in the day deep trawls. Of the 77 cephalopod taxa reported from the
594 region of the Madagascar Ridge (Laptikhovsky et al., 2017), our study sampled only 17 taxa
595 at both La Pérouse and MAD-Ridge seamounts, largely under sampling this broad category.
596 Squids are also relatively weak acoustic targets at 38 kHz (Simmonds & MacLennan, 2005)
597 and studies commonly used a combination of frequencies to locate squid schools (Starr and
598 Thorne, 1998). Of the 32 species of decapods and lophogastrids reported from the
599 Madagascar Ridge, (Letessier et al., 2017), only 16 and 13 crustacean taxa were correctly

identified at La Pérouse and MAD-Ridge respectively. Studies have found elevated abundances of crustacean taxa in the vicinity of seamounts of the South West Indian Ridge and have concluded that some taxa may resist advective lost from seamounts by active migration (Letessier et al., 2017). These taxa were reported to support rich communities of benthopelagic fishes living close to the bottom of the ridge (Vereshchaka et al., 1995).

While *D. suborbitalis*, *N. macrolepidotus* and *B. fibulatum* are diel vertical migrants, associated with the summit and flanks of seamounts but can also be found in the open ocean at the seamount's vicinity, the non-migrant benthopelagic fish species *C. japonicus* and larvae from the Priacanthidae family, were exclusively caught over the summit of MAD-Ridge and were hence truly resident at the seamount. Large populations of *D. suborbitalis* have previously been found to be associated with the Equator seamount (close to the shallow peak called Travin Bank) in the Indian Ocean (Parin & Prut'ko, 1985; Porteiro & Sutton, 2007). These fishes were reported to be located on the slopes at 500-600 m depth during daylight hours and to ascend in dense schools to 80-150 m depth at night for feeding on oceanic plankton, mainly copepods (Gorelova & Prut'ko, 1985), while at the same time being preyed upon by several top predators such as tunas and swordfish (Parin & Prut'ko, 1985). The fish *B. fibulatum* was found to be associated with the Hawaiian Cross seamount summit (330 m below the sea surface) in the Pacific (De Forest & Drazen, 2009), but abundance estimates at the seamount depended largely on lunar illumination (Drazen et al., 2011).

4.5 Do seamounts have higher abundance/biomasses/densities over the summit?

The physical obstruction created by a seamount has been hypothesized to reduce the density of animals over the flanks and summits, particularly at night (eg. Genin et al., 1988; Diekmann et al., 2006; De Forest & Drazen, 2009), hence the lower abundance/biomass estimates of micronekton over the summit compared to the immediate vicinity. However,

624 gas-bearing seamount-associated/resident fauna including *D. suborbitalis*, *N. macrolepidotus*,
625 *B. fibulatum*, *C. japonicus* (MAD-Ridge) and *D. suborbitalis* (La Pérouse), might have
626 formed dense aggregations below the SSL, in close proximity to the summits and flanks
627 (hence the "white patches" seen on RGB composites). The densities and/or target strengths of
628 these organisms are high. These high acoustic detections might also have been caused by
629 deep-water fish aggregations (more commonly described as "plumes") (Bull et al., 2001;
630 O'Driscoll et al., 2012) that were not sampled by the IYGPT net. Fish species such as orange
631 roughy which are commercially fished at Walter Shoals along the Madagascar Ridge
632 (Collette & Parin, 1991), are poor acoustic targets due to their oil-filled swimbladders and are
633 known to avoid mesopelagic trawls (Kloser et al., 2002). The plume peaks that rose above the
634 summits of La Pérouse and MAD-Ridge seamounts into the water column might have been
635 caused by horizontal fish movements from elsewhere on the seamount or vertical movements
636 when fish moved in the water column (O'Driscoll et al., 2012). These plumes may represent
637 aggregations of seamount-resident fishes that avoided advective loss from the seamount and
638 formed dense aggregations over the summits and flanks. In the open ocean such as the South
639 Mozambique Channel, micronekton were more dispersed in the water column since no dense
640 aggregations ("white patches") were observed.

641 Organisms may associate with the La Pérouse and MAD-Ridge seamounts: (1) to increase
642 feeding efficiency (Vereshchaka et al., 1995; Wilson & Boehlert, 2004), (2) to take advantage
643 of a broader range of habitat diversity created by the topography (Wilson & Boehlert, 2004;
644 Porteiro & Sutton, 2007) such as shelter regions for spawning, and (3) to decrease energy loss
645 by using this habitat as a shelter during non-feeding intervals whereby in the open ocean
646 organisms may have to swim constantly. Annasawmy et al., (2019a) showed these seamount-
647 associated fishes to prey on calanoida and chaetognatha at the MAD-Ridge summit and to
648 display similar trophic levels irrespective of their body sizes, confirming the importance of

649 MAD-Ridge seamount as a feeding ground for some mesopelagic/benthopelagic taxa.
650 Benthopelagic animals (such as *C. japonicus*) were reported to prefer rocky seabeds and may
651 take advantage of strong currents over seamounts for advection of their main prey items
652 while avoiding being swept from the summit by using rocky canyons within the seamount
653 topography as shelter regions (Vereshchaka et al., 1995).

654 The reasons for the observed variability in mean backscatter at MAD-Ridge summit
655 compared to the immediate vicinity and the reasons for the observed decrease in trawl
656 abundance/biomass estimates at the summit are further discussed with respect to the sampling
657 strategy and IYGPT net used. Although trawl surveys are necessary to determine the
658 taxonomic composition of micronekton present in the water column in space and time, the
659 composition and biomass obtained largely depend on the type of trawl used (Kwong et al.,
660 2018), their catchability towards various taxonomic groups of nekton and the depth range
661 sampled. Trawl sampling is difficult on shallow topographies because of the high risk of
662 damaging the sampling gear (Christiansen et al., 2009). Hence, the time spent surveying the
663 summit is generally limited. The trawls #14, 15 and 16 over the summit and flanks of MAD-
664 Ridge were directed to specifically sample dense aggregations observed by acoustics and
665 hence the trawl had failed to capture the full suite of organisms present at the study sites.
666 While trawl surveys are useful in terms of the determination of the species composition and
667 assemblages of micronekton, they are also generally expensive, time-consuming and allow a
668 relatively limited collection of samples at any given area. Trawl catches provide only a
669 snapshot of the communities dwelling at seamounts which depends strongly on the time of
670 day and the sampling depths.

671 Active acoustics, on the other hand, while not being able to correctly resolve the taxonomic
672 composition of the micronekton fauna yet, provide continuous measurements of the
673 mesopelagic layer and can be used to determine organisms' abundances/densities,

movements and migrations at various spatial and temporal scales. The combination of active acoustics with trawl and Scanmar data in the form of RGB composites provide invaluable insights into the distributions, the depths of the different scattering layers, the scattering properties of organisms and can be used to speculate about organisms' aggregating behaviour. Kloser et al. (2002) used a similar approach, but the composite image was produced by assigning a separate colour palette to each frequency (12 kHz, 38 kHz and 120 kHz) and dynamically optimising the frequencies to highlight the amplitude differences in the echogram. Our RGB composite approach has the added advantage of further highlighting the presence of structures under-sampled by trawls due to their patchy distribution ("blue patches" with a high frequency response to the 120 kHz; Fig. 10d, Trawl #21 at ~30m) and that could be further investigated using multi-frequency classification.

Due to the successful collection of mesopelagic organisms that can be used to ground-truth the biological scatterers observed under acoustics, our future work will focus on multi-frequency classification to better discriminate sound scatterers, thus allowing us to investigate the relative composition and density of the most common micronekton taxa across the whole cruises where trawl data are missing. This study allowed accurate visual observations of communities present over seamounts at the time of the cruises and will allow the development of accurate schematics, representing the various DVM strategies and the different scattering properties of the micronekton broad categories (gelatinous organisms, crustaceans, cephalopods and fishes) in the open ocean, on the flanks and summits of seamounts.

Concluding remarks

We used a combination of datasets (active acoustics and mesopelagic trawls) to investigate the dynamics of micronekton at two shallow seamounts. The eddy dynamics, advection of

productivity from the Madagascar landmass and connectivity with neighbouring seamounts and landmasses may result in greater micronekton species richness at MAD-Ridge compared to La Pérouse which is located in an oligotrophic environment. As topographic obstacles, seamounts may have an impact on the vertical distribution of micronekton by temporarily halting the latter in their upward and downward migrations. The night SSL (between 10-200 m) over the summit and flanks concentrated common open-water species of gelatinous (salps and pyrosomes), crustaceans (Euphausiacea sp., *Funchalia* sp. and phyllosoma larvae), squids (Enoploteuthidae sp., *C. scabra* and *Abraliopsis* sp.), and fishes (leptocephali larvae, *H. hygomii* and various species of *Diaphus* sp.). In addition to the vertically migrant organisms forming the SSL, we provided evidence that La Pérouse and MAD-Ridge seamounts support an important community of seamount-associated/resident fishes (La Pérouse and MAD-Ridge: *D. suborbitalis*; MAD-Ridge: *B. fibulatum* and *C. japonicus*) that occur in dense aggregations over the summits and flanks. Despite several shortcomings in this work, notably during La Pérouse and MAD-Ridge cruise sampling, this study fills an important knowledge gap. The combined use of satellite, mesopelagic trawl and acoustic data at the time of the cruises, provides an integrative and accurate picture as to the mechanisms involved in micronekton vertical/horizontal distributions and assemblages at shallow topographies. More importantly, this study helps contribute to our growing understanding of seamount ecosystems in the south-western Indian Ocean. Improving our knowledge of the ecosystems associated to shallow seamounts is a key issue towards the promotion of specific sustainable use and conservation measures dedicated to protecting such critical environments.

Acknowledgement

The authors acknowledge the work carried by the non-scientific staff on board the R.V. *ANTEA* and the scientific staff who participated in the data acquisition and data processing, including Delphine Thibault (MIO, Marseille, France), P. Alexander Hulley (South Africa)

723 for confirming the taxonomy of the micronekton taxa and Hervé Demarcq (IRD, Sète,
724 France) for providing the SSC data. This study was mainly supported by the Flotte
725 Océanographique Française (French Oceanographic Fleet) and IRD in relation to the logistics
726 of the R.V. *ANTEA*. Additional funding was received from Région Reunion (Réunion
727 Regional Council) for La Pérouse cruise, and from the Fonds Français pour l'Environnement
728 Mondial (FFEM) as part of the FFEM-SWIO project on Areas Beyond National Jurisdiction
729 (ABNJ) of the South West Indian Ocean for MAD-Ridge cruise. Pavanee Annasawmy is the
730 beneficiary of a doctoral bursary granted by the Institut de Recherche pour le Développement
731 (IRD, France) and the ICEMASA French-South African International Laboratory.

References

Adduce, C., Cenedese, C., 2004. An experimental study of a mesoscale vortex colliding with topography of varying geometry in a rotating fluid. J. Mar. Res. 62, 611-638. https://doi.org/10.1357/0022240042387583

Aksnes, D. L., Røstad, A., Kaartvedt, S., Martinez, U., Duarte, C.M., Irigoien, X., 2017. Light penetration structures the deep acoustic scattering layers in the global ocean. Sci. Adv. 3: e1602468

Alverson, F.G., 1961. Daylight Surface Occurrence of Myctophid Fishes Off the Coast of Central America. Pac Sci. 15(3): 483. http://hdl.handle.net/10125/9088

Andersen, V., François, F., Sardou, J., Picheral, M., Scotto, M., Nival, P., 1998. Vertical distributions of macroplankton and micronekton in the Ligurian and Tyrrhenian Seas (northwestern Mediterranean). Oceanol. Acta 21, 5.

Annasawmy, P., Cherel, Y., Romanov, E., Le Loc'h, F., Ménard, F., Ternon, J.F., Marsac, F., 2019a. Stable isotope patterns of mesopelagic communities over two shallow seamounts of the south-western Indian Ocean. Deep-Sea Res. II, submitted.

Annasawmy, P., Ternon, J-F., Lebourges-Dhaussy, A., Roudaut, G., Herbette, S., Ménard, F., Cotel. P., Marsac, F., 2019c. Micronekton distribution as influenced by mesoscale eddies, Madagascar shelf and shallow seamounts in the south-western Indian Ocean: An acoustic approach. Deep-Sea Res. II-submitted.

Annasawmy, P., Ternon, J.F., Marsac, F., Cherel, Y., Béhagle, N., Roudaut, G., Lebourges-Dhaussy, A., Demarcq, H., Moloney, C.L., Jaquemet, S., Ménard, F., 2018. Micronekton diel migration, community composition and trophic position within two biogeochemical provinces of the South West Indian Ocean: Insight from acoustics and stable isotopes. Deep Sea Research Part I: Oceanographic Research Papers. 138, 85–97. https://doi.org/10.1016/j.dsr.2018.07.002

Ariza, A., Landeira, J.M., Escánez, A., Wienerroither, R., Aguilar de Soto, N., Røstad, A., Kaartvedt, S., Hernández-León, S., 2016. Vertical distribution, composition and migratory patterns of acoustic scattering layers in the Canary Islands. J. Mar. Syst. 157, 82–91. https://doi.org/10.1016/j.jmarsys.2016.01.004

Bashmachnikov, I., Loureiro, C.M., Martins, A., 2013. Topographically induced circulation patterns and mixing over Condor seamount. Deep-Sea Res. II. 98: 38-51. http://dx.doi.org/10.1016/j.dsr2.2013.09.014

Béhagle, N., du Buisson, L., Josse, E., Lebourges-Dhaussy, A., Roudaut, G., Ménard, F., 2014. Mesoscale features and micronekton in Mozambique Channel: An acoustic approach. Deep Sea Res. Part II. 100, 164-173. https://doi.org/10.1016/j.dsr2.2013.10.024

Béhagle, N., Cotté, C., Lebourges-Dhaussy, A., Roudaut, G., Duhamel, G., Brehmer, P., Josse, E., Cherel, Y., 2017. Acoustic distribution of discriminated micronektonic organisms from a bi-frequency processing: the case study of eastern Kerguelen oceanic waters. Prog. Oceanogr. 156, 276-289. https://doi.org/10.1016/j.pocean.2017.06.004

Benoit-Bird, K. J., Lawson, G. L., 2016. Ecological Insights from Pelagic Habitats Acquired Using Active Acoustic Techniques. Annu. Rev. Mar. Sci. 8, 21.1–21.28. https://doi.org/10.1146/annurev-marine-122414-034001

Bensch, A., Gianni, M., Gréboval, D., Sanders, J., Hjort, A., 2009. Worldwide review of bottom fisheries in the high seas. FAO Fisheries and Aquaculture Technical Paper. 522(1). Rome. 145p.

Bernal, A., Olivar, M.P., Maynou, F., Fernández de Puelles, M.L., 2015. Diet and feeding strategies of mesopelagic fishes in the western Mediterranean. Progr. Oceanogr. 135, 1–17. https://doi.org/10.1016/j.pocean.2015.03.005.

Boehlert, G.W., and Genin, A., 1987. A review of the effects of seamounts on biological processes. In: Seamounts, Islands and Atolls (eds. Keating, B.H., Fryer, P., Batiza, R. and Boehlert, G.W.), p. 319–34. Geophysics Monographic Series 43. American Geophysical Union. Washington, DC.

Boersch-Supan, P., Rogers, A.D., Brierley, A.S., 2017. The distribution of pelagic sound scattering layers across the southwest Indian Ocean. Deep-Sea Res. II. 136: 108-121. http://dx.doi.org/10.1016/j.dsr2.2015.06.023

Bograd, S.J., Rabinovich, A.B., LeBlond, P.H., Shore, J.A., 1997. Observations of seamount-attached eddies in the North Pacific. J. Geophys. Res. Oceans. 102, 12441–12456. https://doi.org/10.1029/97JC00585

Brodeur, R., and Yamamura, O., 2005. PICES Scientific Report No. 30 Micronekton of the North Pacific. PICES Scientific Report, Sidney, B.C., Canada, pp. 1–115.

Bull, B., Doonan, I., Tracey, D., Hart, A., 2001. Diel variation in spawning orange roughy (*Hoplostethus atlanticus*, Trachichthyidae) abundance over a seamount feature on the north-west Chatham Rise. New Zealand Journal of Marine and Freshwater Research. 35(3): 435-444. DOI: 10.1080/00288330.2001.9517013

Cascão, I., Domokos, R., Lammers, M.O., Marques, V., Domínguez, R., Santos, R.S., Silva, M.A., 2017. Persistent enhancement of micronekton backscatter at the summits of seamounts in the Azores. Front. Mar. Sci. https://doi.org/10.3389/fmars.2017.00025

Cherel, Y., Fontaine, C., Richard, P., Labat, J-P., 2010. Isotopic niches and trophic levels of myctophid fishes and their predators in the Southern Ocean. Limnol. Oceanogr. 55(1), 324-332. https://doi.org/10.4319/lo.2010.55.1.0324

Cherel, Y., Romanov, E.V., Annasawmy, P., Thibault, D., Ménard, F., 2019. Micronektonic fish species over three seamounts in the southwestern Indian Ocean and myctophid infestation by the copepod *Cardiodectes bellotti*. Deep-Sea Res. II-submitted.

Christiansen, B., Martin, B., Hirch, S., 2009. The benthopelagic fish fauna on the summit of Seine seamount, NE Atlantic: Composition, population structure and diets. Deep Sea Res. Part II. 56(25), 2705-2712. https://doi.org/10.1016/j.dsr2.2008.12.032

Clark, M.R., Vinnichenko, V.I., Gordon, J.D.M., Beck-Bulat, G.Z., Kukharev, N.N., Kakora, A.F., 2007. Large-scale distant-water trawl fisheries on seamounts. In: Pitcher, T.J., Morato, T., Hart, P.J.B., Clark, M.R., Haggan, N., Santos, R.S. (Eds.), Seamounts: Ecology, Fisheries & Conservation. Blackwell Publishing Ltd, Oxford, UK, pp. 361–399. https://doi.org/10.1002/9780470691953.ch4

Clarke, M.R., Lu, C.C., 1975. Vertical distribution of cephalopods at 18°N 25°W in the North Atlantic. J. mar. biol. Ass. 55: 165-182. https://doi.org/10.1017/S0025315400015812

Clarke, K. R., Warwick, R. M., 2001. Change in marine communities: an approach to statistical analysis and interpretation, 2nd edition. PRIMER-E, Plymouth, UK.

Cohen, J.H., Forward, R.B., 2009. Zooplankton diel vertical migration- a review of proximate control. Oceanography and marine biology. 47: 77-109. DOI: 10.1201/9781420094220.ch2

Collette, B.B., Parin, N.V., 1991. Shallow-water fishes of Walters Shoals, Madagascar Ridge. Bulletin of Marine Science. 48(1):1-22.

Danckwerts, D.K., McQuaid, C.D., Jaeger, A., McGregor, G.K., Dwight, R., Le Corre, M., Jaquemet, S., 2014. Biomass consumption by breeding seabirds in the western Indian Ocean: indirect interactions with fisheries and implications for management. ICES Jour. of Mar. Sci. 71(9), 2589-2598. https://doi.org/10.1093/icesjms/fsu093

Davison, P. C., Koslow, J. A., Kloser, R. J., 2015. Acoustic biomass estimation of mesopelagic fish: backscattering from individuals, populations, and communities. ICES Jour. Mar. Sci. 72(5), 1413-1424. https://doi.org/10.1093/icesjms/fsv023

De Forest, L., Drazen, J., 2009. The influence of a Hawaiian seamount on mesopelagic micronekton. Deep Sea Res Part I. 56(2), 232-250. https://doi.org/10.1016/j.dsr.2008.09.007

De Robertis, A., Higginbottom, I., 2007. A post-processing technique to estimate the signal-to-noise ratio and remove echosounder background noise. ICES Jour. Mar. Sci. 64, 1282-1291. https://doi.org/10.1093/icesjms/fsm112

Diekmann, R., Nellen, W., Piatkowski, U., 2006. A multivariate analysis of larval fish and paralarval cephalopod assemblages at Great Meteor Seamount. Deep-Sea Res. I. 53: 1635-1657. DOI:10.1016/j.dsr.2006.08.00

Domokos, R., Pakhomov, E.A., Suntsov, A.V., Seki, M.P., Polovina, J.J., 2010. PICES Scientific Report. No. 38. Acoustic characterization of the mesopelagic community off the leeward coast of Oahu Island, Hawaii. E. A. Pakhomov, O. Yamamura (Eds.), Report of the Advisory Panel on Micronekton Sampling Intercalibration Experiment.pp 19-26.

Drazen, J. F., De Forest, L. G., Domokos, R., 2011. Micronekton abundance and biomass in Hawaiian waters as influenced by seamounts, eddies and the moon. Deep Sea Res Part I. 58, 557-566. http/doi.org/10.1016/j.dsr.2011.03.002

Dubroca, L., Chassot, E., Floch, L., Demarcq, H., Assan, C., Delgado de Molina, A., 2013. Seamounts and tuna fisheries: Tuna hotspots or fishermen habits? Collect. Vol. Sci. Pap. ICCAT. 69(5), 2087-2102.

Dulau, V., Pinet, P., Geyer, Y., Fayan, J., Mongin, P., Cottarel, G., Zerbini, A., Cerchio, S., 2017. Continuous movement behavior of humpback whales during the breeding season in the southwest Indian Ocean: on the road again! Movement Ecology. 5(11):2-17. DOI: 10.1186/s40462-017-0101-5

Ekau, W., Auel, H., Pörtner, H.-O., Gilbert, D., 2010. Impacts of hypoxia on the structure and processes in pelagic communities (zooplankton, macro-invertebrates and fish). Biogeosciences 7, 1669–1699. https://doi.org/10.5194/bg-7-1669-2010.

Fennell, S., Rose, G., 2015. Oceanographic influences on Deep Scattering Layers across the North Atlantic. Deep-Sea Res I. 105: 132-141. http://dx.doi.org/10.1016/j.dsr.2015.09.002

Foote, K. G., Knudsen, H. P., Vestnes, G., MacLennan, D. N., Simmonds, E. J., 1987. Calibration of acoustic instruments for fish density estimation: a practical guide. ICES Coop. Res. Rep. 144, 1-69.

Fonteneau, A. 1991. Monts sous-marins et thons dans l'Atlantique tropical est. Aquat. Living Resour. 4, 13-25.

Freeland, H., 1994. Ocean circulation at and near Cobb Seamount. Deep-Sea Res. I. 41(11/12): 1715-1732.

Fréon, P., and Dagorn, L., 2000. Review of fish associative behaviour: Toward a generalisation of the meeting point hypothesis. Reviews in Fish Biology and Fisheries. 10, 183-207. DOI: 10.1023/A:1016666108540

Furusawa, M., Miyanohana, Y., Ariji, M., Sawada, Y., 1994. Prediction of krill target strength by liquid prolate spheroid model. Fisheries Science. 60(3): 261-265.

Genin, A., Haury, L., Greenblatt, P., 1988. Interactions of migrating zooplankton with shallow topography: predation by rockfishes and intensification of patchiness. Deep-Sea Res. 35(2): 151-175.

Genin, A., 2004. Bio-physical coupling in the formation of zooplankton and fish aggregations above adrupt topographies. J. Mar. Syst. 50, 3-20.

https://doi.org/10.1016/j.jmarsys.2003.10.008
Gjosaeter, J., 1978. Aspects of the distribution and ecology of the Myctophidae from the Western and Northern Arabian Sea. Development Report Indian Ocean Programme, 43: 62–108.
Gjosaeter, J., 1984. Mesopelagic fish, a large potential resource in the Arabian Sea. Deep-Sea Res. Part A. 31:1019–1035.
Gorelova, T. A., and Prut′ko, V. G., 1985. Feeding of *Diaphus suborbitalis* (Myctophidae, Pisces) in the Equatorial Indian Ocean. Okeanologiya, Academy of Sciences of the USSR, (25): 523-529
Guinet, C., Cherel, Y., Ridoux, V., Jouventin, P., 1996. Consumption of marine resources by seabirds and seals in Crozet and Kerguelen waters: changes in relation to consumer biomass 1962-85. Antarctic Sci. 8(1), 23-30. https://doi.org/10.1017/S0954102096000053
Herbette, S., Morel, Y., Arhan, M., 2003. Erosion of a surface vortex by a seamount. Journal of Physical Oceanography. 33(1), 664-679. https://doi.org/10.1175/2382.1
Hirch, S., Christiansen, B., 2010. The trophic blockage hypothesis is not supported by the diets of fishes on Seine seamount. Mar. Ecol. 31(Suppl. 1): 107-120. DOI:10.1111/j.1439-0485.2010.00366.x
Holland, K. N., and Grubbs, R. D., 2007. Fish visitors to seamounts: Tunas and billfish at seamounts. In Seamounts: Ecology, Fisheries and Conservation. 189-201. https://doi.org/10.1002/9780470691953.ch10a.
Ingole, B., Koslow, J.A., 2005. Deep-sea ecosystems of the Indian Ocean. Indian Journal of Marine Sciences. 34(1): 27-34.
Isaacs, J. D., Schwartzlose, R. A., 1965. Migrant sound scatterers: Interaction with the sea floor. Science. 150(3705), 1810-1813. https://doi.org/10.1126/science.150.3705.1810
Jaquemet, S., Ternon, J. F., Kaehler, S., Thiebot, J. B., Dyer, B., Bemanaja, E., Marteau, C., Le Corre, M., 2014. Contrasted structuring effects of mesoscale features on the seabird communities in the Mozambique Channel. Deep Sea Res Part II. 100, 200-211. http://dx.doi.org/10.1016/j.dsr2.2013.10.027
Johnston, D. W., McDonald, M., Polovina, J., Domokos, R., Wiggins, S., Hildebrand, J., 2008. Temporal patterns in the acoustic signals of beaked whales at Cross Seamount. Biol. Lett. 4, 208–211. https://doi.org/10.1098/rsbl.2007.0614
Judkins, D.C., and Haedrich, R.L., 2018. The deep scattering layer micronektonic fish faunas of the Atlantic mesopelagic ecoregions with comparison of the corresponding decapod shrimp faunas. Deep Sea Res. Part I. https://doi.org/10.1016/j.dsr.2018.04.008
Kaartvedt, S., Klevjer, T.A., Aksnes, D.L., 2012. Internal wave-mediated shading causes frequent vertical migrations in fishes. Mar. Ecol. Prog. Ser. 452: 1-10. DOI: 10.3354/meps09688
Kloser, R. J., Ryan, T., Sakov, P., Williams, A., Koslow, J. A., 2002. Species identification in deep water using multiple acoustic frequencies. Can. J. Fish. Aquat. Sci. 59, 1065–1077. https://doi.org/10.1139/f02-076
Kloser, R. J., Ryan, T. E., Young, J. W., Lewis, M. E., 2009. Acoustic observations of micronekton fish on the scale of an ocean basin: potential and challenges. ICES Jour. Mar. Sci. 66(6), 998-1006. https://doi.org/10.1093/icesjms/fsp077
Kloser, R.J., Ryan, T.E., Keith, G., Gershwin, L., 2016. Deep-scattering layer, gas-bladder density, and size estimates using a two-frequency acoustic and optical probe. ICES J Mar Sci. 73(8): 2037-2048. DOI:10.1093/icesjms/fsv257
Kolasinski, J., Kaehler, S., Jaquemet, S., 2012. Distribution and sources of particulate organic matter in a mesoscale eddy dipole in the Mozambique Channel (south-western Indian

Ocean): Insight from C and N stable isotopes. J. Mar. Syst. 96-97, 122-131. https://doi.org/10.1016/j.jmarsys.2012.02.015

Kwong, L.E., Pakhomov, E.A., Suntsov, A.V., Seki, M.P., Brodeur, R.D., Pakhomova, L.G., Domokos, R., 2018. An intercomparison of the taxonomic and size composition of tropical macrozooplankton and micronekton collected using three sampling gears. Deep Sea Res. Part I. https://doi.org/10.1016/j.dsr.2018.03.013

Lack, M., Short, K., Willock, A., 2003. Managing risk and uncertainty in deep-sea fisheries: lessons from Orange Roughy. TRAFFIC Oceania and WWF Endangered Seas Programme.

Laptikhovsky, V., Boersch-Supan, P., Bolstad, K., Kemp, K., Letessier, T., Rogers, A.D., 2017. Cephalopods of the Southwest Indian OceanRidge: A hotspot of biological diversity and absence of endemism. Deep-Sea Res II. 136: 98-107. http://dx.doi.org/10.1016/j.dsr2.2015.07.002

Lavelle, J. W., Mohn, C., 2010. Motion, commotion, and biophysical connections at deep ocean seamounts. Oceanography. 23(1), 90-103. https://doi.org/10.5670/oceanog.2010.64

Lebourges-Dhaussy, A., Marchal., E., Menkès, C., Champalbert, G., Biessy, B., 2000. *Vinciguerria nimbaria* (micronekton), environment and tuna: their relationships in the eastern Tropical Atlantic. Oceanologica Acta. 23(4), 515-528. https://doi.org/10.1016/S0399-1784(00)00137-7

Lehodey, P., Murtugudde, R., Senina, I., 2010. Bridging the gap from ocean models to population dynamics of large marine predators: A model of mid-trophic functional groups. Prog. in Oceanography. 84: 69-84. DOI:10.1016/j.pocean.2009.09.008

Letessier, T.B., Cox, M.J., Meeuwig, J.J., Boersch-Supan, P.H., Brierley, A.S., 2015. Enhanced pelagic biomass around coral atolls. Mar. Ecol. Prog. Ser. 546: 271-276. DOI: 10.3354/meps11675

Letessier, T.B., De Grave, S., Boersch-Supan, P.H., Kemp, K.M., Brierley, A.S., Rogers, A.D., 2017. Seamount influences on mid-water shrimps (Decapoda) and gnathophausiids (Lophogastridea) of the South-West Indian Ridge. Deep-Sea Res. II. 136: 85-97. http://dx.doi.org/10.1016/j.dsr2.2015.05.009

Longhurst, A., 2007. Ecological geography of the sea. 2nd edition. San Diego, CA: Academic Press.

MacLennan, D. N., Fernandes, P. G., Dalen, J., 2002. A consistent approach to definitions and symbols in fisheries acoustics. ICES Jour. Mar. Sci. 59, 365-369. https://doi.org/10.1006/jmsc.2001.1158

Marchal, E., Lebourges-Dhaussy, A., 1996. Acoustic evidence for unusual diel behaviour of a mesopelagic fish (*Vinciguerria nimbaria*) exploited by tuna. ICES J. Mar. Sci. 53, 443–447. https://doi.org/10.1006/jmsc.1996.0062

Marsac, F., Fonteneau, A., Michaud, P., 2014. Le « Coco de Mer », une montagne sous la mer. In: L'or bleu des Seychelles: Histoire de la pêche industrielle au thon dans l'océan Indien. IRD Editions, pp 151- 163.

McClatchie, S., Coombs, R.F., 2005. Low target strength fish in mixed species assemblages: the case of orange roughy. Fisheries Research. 72: 185-192. DOI:10.1016/j.fishres.2004.11.008

Mohn, C., Beckmann, A., 2002. The upper ocean circulation at Great Meteor Seamount. Ocean Dyn. 52, 179–193. https://doi.org/10.1007/s10236-002-0017-4

Mohn, C., White, M., Bashmachnikov, I., Jose, F., Pelegri, J.L., 2009. Dynamics at an elongated, intermediate depth seamount in the North Atlantic (Sedlo Seamount, 40°20'N, 26°40'W). Deep-Sea Res. II. 56: 2582-2592. DOI:10.1016/j.dsr2.2008.12.037

Morato, T., Varkey, D. A., Damaso, C., Machete, M., Santos, M., Prieto, R., Santos, R. S., and Pitcher, T. J., 2008. Evidence of a seamount effect on aggregating visitors. Mar Ecol Prog Ser. 357, 23-32. https://doi.org/10.3354/meps07269

Nesis, K., 1993. Cephalopods of seamounts and submarine ridges. In: Okutani, T., O'Dor, R.K., Kubodera, T. (Eds.), Recent Advances in Cephalopod Fisheries Biology. Tokai University Press, Tokyo, Japan, pp. 365–374.

O'Driscoll, R., De Joux, P., Nelson, R., Macaulay, G.J., Dunford, A.J., Marriott, P.M., Stewart, C., Miller, B.S., 2012. Species identification in seamount fish aggregations using moored underwater video. ICES Journal of Marine Science. 69(4): 648-659. DOI:10.1093/icesjms/fss010

Oksanen, J., Blanchet, F. G., Friendly, M., Kindt, R., Legendre, P., McGlinn, D., Minchin, P. R., O'Hara, R. B., Simpson, G. L., Solymos, P., Stevens, M. H. H., Szoecs, E., Wagner, H., 2018. Package 'vegan': Community Ecology Package, R package version 2.5-1.
https://CRAN.R-project.org/package=vegan

Olivar, M.P., Bernal, A., Molí, B., Peña, M., Balbín, R., Castellón, A., Miquel, J., Massutí, E., 2012. Vertical distribution, diversity and assemblages of mesopelagic fishes in the western Mediterranean. Deep Sea Res. Part I 62, 53–69.

Olivar, M.P., Hulley, P.A., Castellón, A., Emelianov, M., López, C., Tuset, V.M., Contreras, T., Molí, B., 2017. Mesopelagic fishes across the tropical and equatorial Atlantic: biogeographical and vertical patterns. Progr. Oceanogr. 151, 116–137.

Owens, W.B., Hogg, N.G., 1980. Oceanic observations of stratified Taylor columns near a bump. Deep-Sea Res. 27A: 1029-1045.

Parin, N. V., and Prut'ko, V. G., 1985. Thalassal mesobenthopelagic ichthyocoenosis above the Equator Seamount in the western tropical Indian Ocean. Okeanologiya, Academy of Sciences of the USSR, 25(6): 1017-1020.

Parin, N.V., Timokhin, I.G., Novikov, N.P., Shcherbachev, Y.N., 2008. On the composition of talassobathyal ichthyofauna and commercial productivity of Mozambique Seamount (the Indian Ocean). Journal of Ichthyology. 48(5): 361-366.
https://doi.org/10.1134/S0032945208050019

Pearcy, W.G., Krygier, E.E., Mesecar, R., Ramsey, F., 1977. Vertical distribution and migration of oceanic micronekton off Oregon. Deep-Sea Res. 24: 223-245.

Perrot, Y., Brehmer, Y., Habasque, J., Roudaut, G., Béhagle, N., Sarré, A., Lebourges-Dhaussy, A., 2018. Matecho: An open-source tool for processing fisheries acoustics data. Acoust Aust. https://doi.org/10.1007/s40857-018-0135-x

Pollard, R., Read, J., 2015. Circulation, stratification and seamounts in the Southwest Indian Ocean. Deep Sea Res Part II Top. Stud. Oceanogr. 136, 36-43. https://doi.org/10.1016/j.dsr2.2015.02.018

Porteiro, F.M., and Sutton, T., 2007. Midwater Fish Assemblages and Seamounts, in: Pitcher, T.J., Morato, T., Hart, P.J.B., Clark, M.R., Haggan, N., Santos, R.S. (Eds.), Seamounts: Ecology, Fisheries & Conservation. Blackwell Publishing Ltd, Oxford, UK, pp. 101–116. https://doi.org/10.1002/9780470691953.ch6

Potier, M., Marsac, F., Lucas, V., Sabatié, R., Hallier, J-P., Ménard, F., 2004. Feeding partitioning among tuna taken in surface and mid-water layers: The case of Yellowfin (*Thunnus albacares*) and Bigeye (*T. obesus*) in the Western Tropical Indian Ocean. Western Indian Ocean J. Mar. Sci. 3(1), 51-62.

Potier, M., Marsac, F., Cherel, Y., Lucas, V., Sabatié, R., Maury, O., Ménard, F., 2007. Forage fauna in the diet of three large pelagic fishes (lancetfish, swordfish and yellowfin tuna) in the western equatorial Indian Ocean. Fisheries Research. 83, 60-72. http://doi.org/10.1016/j.fishres.2006.08.020

Potier, M., Bach, P., Ménard, F., Marsac, F., 2014. Influence of mesoscale features on micronekton and large pelagic fish communities in the Mozambique Channel. Deep Sea Res Part II Top. Stud. Oceanogr. 100, 184-199. http://dx.doi.org/10.1016/j.dsr2.2013.10.026

Proud, R., Cox, M. J., Brierley, A. S., 2017. Biogeography of the global ocean's mesopelagic zone. Current Biology. 27, 113-119. http://dx.doi.org/10.1016/j.cub.2016.11.003

Proud, R., Handegard, N. O., Kloser, R. J., Cox, M. J., Brierley, A. S., 2018. From siphonophores to deep scattering layers: uncertainty ranges for the estimation of global mesopelagic fish biomass. ICES J. Mar. Sci. fsy037. https://doi.org/10.1093/icesjms/fsy037

Quartly, G. D., and Srokosz, M. A., 2004. Eddies in the southern Mozambique Channel. Deep Sea Res Part II Top. Stud. Oceanogr. 51, 69-83. https://doi.org/10.1016/j.dsr2.2003.03.001

Ramanantsoa, J. D., Krug, M., Penven, P., Rouault, M., Gula, J., 2018. Coastal upwelling south of Madagascar: Temporal and spatial variability. J. Mar. Syst. 178, 29-37. http://dx.doi.org/10.1016/j.jmarsys.2017.10.005

Read, J., Pollard, R., 2017. An introduction to the physical oceanography of six seamounts in the southwest Indian Ocean. Deep-Sea Res. II. 136: 44-58. https://doi.org/10.1016/j.dsr2.2015.06.022

Reid, S.B., Hirota, J., Young, R.E., Hallacher, L.E., 1991. Mesopelagic-boundary community in Hawaii: micronekton at the interface between neritic and oceanic ecosystems. Mar. Biol. 109: 427-440.

Rogers, A.D., Bemanaja, O.A.E., Benivary, D., Boersch-Supan, P., Bornman, T.G., Cedras, R., Du Plessis, N., Gotheil, S., Høines, A., Kemp, K., Kristiansen, J., Letessier, T., Mangar, V., Mazungula, N., Mørk, T., Pinet, P, Pollard, R., Read, J., Sonnekus, T., 2017. Pelagic communities of the South West Indian Ocean seamounts: R/V Dr *Fridtjof* Nansen Cruise 2009-410. Deep Sea Res. II. 136: 5-35. https://doi.org/10.1016/j.dsr2.2016.12.010

Romanov, E.V., (2003). Summary and review of Soviet and Ukrainian scientific and commercial fishing operations on the deepwater ridges of the southern Indian Ocean. FAO Fisheries Circular. No. 991. Rome, FAO. 84p.

Romero-Romero, S., Choy, C.A., Hannides, C.C.S., Popp, B.N., Drazen, J.C., 2019. Differences in the trophic ecology of micronekton driven by diel vertical migration. Limnol. Oceanogr. 9999:1-11. DOI: 10.1002/lno.11128

Royer, T.C., 1978. Ocean eddies generated by seamounts in the North Pacific. Science. 199, 1063–4.

Ryan, T. E., Downie, R. A., Kloser, R. J., Keith, G., 2015. Reducing bias due to noise and attenuation in open-ocean echo integration data. ICES Jour. Mar. Sci. 72, 2482-2493. https://doi.org/10.1093/icesjms/fsv121

Sabarros, P.S., Ménard, F., Lévénez, J-J., Tew-Kai, E., Ternon, J-F., 2009. Mesoscale eddies influence distribution and aggregation patterns of micronekton in the Mozambique Channel. Mar Ecol Prog Ser. 395: 101-107. DOI: 10.3354/meps08087

Schouten, M. W., De Ruijter, W. P. M., van Leeuwen, P. J., 2000. Translation, decay and splitting of Agulhas rings in the southeastern Atlantic Ocean. JGR. 105(9), 21913-21925. https://doi.org/10.1029/1999JC000046

Simmonds, J., MacLennan, D., 2005. Fisheries Acoustics: theory and practice. Second Edition. Blackwell Science, Oxford, UK. 437 pp.

Smith, M.M., Heemstra, P.C., 1986. Smith's Sea Fishes. J.L.B. Smith Institute of Ichthyology, Grahamstown, South Africa. 1047 p.

Starr, R.M., Throne, R.E., 1998. Acoustic assessment of squid stocks. FAO Fisheries Technical Paper, 181-198.

Sutyrin, G. G., 2006. Critical effects of a tall seamount on a drifting vortex. J. Mar. Res. 64(2), 297-317. https://doi.org/10.1357/002224006777606489

Swart, N. C., Lutjeharms, J. R. E., Ridderinkhof, H., de Ruijter, W. P. M., 2010. Observed characteristics of Mozambique Channel eddies. J. Geophys. Res. 115, C09006/1-C09006/14. https://doi.org/10.1029/2009JC005875

Tew-Kai, E., and Marsac, F., 2009. Patterns of variability of sea surface chlorophyll in the Mozambique Channel: A quantitative approach. J. Mar. Sys. 77, 77-88. https://doi.org/10.1016/j.jmarsys.2008.11.007

Tracey, D. M., Clark, M. R., Anderson, O. F., Kim, S. W., 2012. Deep-sea fish distribution varies between seamounts: Results from a seamount complex off New Zealand. PLOS One. 7(6). https://doi.org/10.1371/journal.pone.0036897

Trenkel, V. M., Berger, L., Bourguignon, S., Doray, M., Fablet, R., Massé, J., Mazauric, V., Poncelet, C., Quemener, G., Scalabrin, C., Villalobos, H., 2009. Overview of recent progress in fisheries acoustics made by Ifremer with examples from the Bay of Biscay. Aquatic Living Res. 22, 433–445. https://doi.org/10.1051/alr/2009027

Van der Spoel, S., Bleeker, J., 1991. Distribution of Myctophidae (Pisces, Myctophiformes) during the four seasons in the mid North Atlantic. Contributions to Zoology. 61(2): 89-106.

Vereshchaka, A.L., 1995. Macroplankton in the near-bottom layer of continental slopes and seamounts. Deep-Sea Res. I. 42(9): 1639-1668.

Vianello, P., Ternon, J-F., Herbette, S., Demarcq, H., Roberts, M.J., 2019. Circulation and hydrography in the vicinity of a shallow seamount on the northern Madagascar Ridge. Deep-Sea Res. II-submitted

Wagawa, T., Yoshikawa, Y., Isoda, Y., Oka, E., Uehara, K., Nakano, T., Kuma, K., Takagi, S., 2012. Flow fields around the Emperor Seamounts detected from current data. Journal of Geophysical Research. 117(C06006). DOI: 10.1029/2011JC007530

Watanabe, H., Kawaguchi, K., Hayashi, A., 2002. Feeding habits of juvenile surface-migratory myctophid fishes (family Myctophidae) in the Kuroshio region of the western North Pacific. Mar. Ecol. Progr. Ser. 236: 263-272.

White, M., Bashmachnikov, I., Arstegui, J., Martins, A., 2007. Physical Processes and Seamount Productivity. In: Pitcher, T.J., Morato, T., Hart, P.J.B., Clark, M.R., Haggan, N., Santos, R.S. (Eds.), Seamounts: Ecology, Fisheries & Conservation. Blackwell Publishing Ltd, Oxford, UK, pp. 62–84. https://doi.org/10.1002/9780470691953.ch4

Wilson, C.D., and Boehlert, G.W., 2004. Interaction of ocean currents and resident micronekton at a seamount in the central North Pacific. J. Mar. Syst. 50, 39–60. https://doi.org/10.1016/j.jmarsys.2003.09.013

Youngbluth, M.J., 1975. The vertical distribution and diel migration of euphausiids in the central waters of the eastern South Pacific. Deep-Sea Res. 22, 519–536. https://doi.org/10.1016/0011-7471(75)90033-9.

List of tables and figures:

abundance of common (c) deep dwelling, (d) and seamount flank associated species. Trawl stations are numbered 1 to 10 on the bubble plots and the 40% similarity clusters are denoted by dotted lines. The larger the bubble, the greater the number of individuals captured at that trawl station.

Figure 8(a) Similarity cluster dendrogram of species abundance at MAD-Ridge trawl stations 1 to 17. Brackets represent cluster groups at 35% (Night shallow, vicinity and flank; Day deep, vicinity and flank); and 30% similarities (Night shallow, summit and flank). b) Schematic diagram of MAD-Ridge seamount. Pie charts represent the abundance and biomass of micronekton (gelatinous organisms in blue, crustaceans in orange, cephalopods in violet and fishes in yellow) within the cluster groups. (c-e) Bubble plot overlays of the MDS ordination representing the relative abundance of common (c) shallow-dwelling and vertical migratory fish species, (d) deep-dwelling, (e) and seamount summit and flank associated fish species. Trawl stations are numbered 1 to 17 on the bubble plots and the 35% and 30% similarity clusters are denoted by dotted lines. The larger the bubble, the greater the number of individuals captured at that trawl station.

Figure 9 Schematics of (a) La Pérouse, and (b) MAD-Ridge seamounts listing the most dominant taxa (gelatinous organisms in blue, crustaceans in orange, cephalopods in violet and fishes in yellow) within the cluster groups. The numbers in brackets indicate the number of individuals caught. Organisms are classified as being epi (epipelagic), meso (mesopelagic), bathy (bathypelagic) and bentho (benthopelagic). Echograms of the 38 kHz frequency at sunset, night, sunrise and daytime are denoted by red, blue, violet and gold coloured rectangles respectively. The successive series of DVM events from the intermediate layer and from the SSL are denoted by circular dotted lines. The night SSL and day SSL are denoted by solid and dotted rectangles respectively. The DSL is denoted by solid rectangles. Seamount-associated species and topographic blockage mechanism are also noted. Colour bar indicates S_V in dB re 1 m^{-1}.

Figure 10 (a-d) RGB composites of S_V values (dB re 1 $m^{-}1$) of trawls 14 and 15 (flank), 16 (summit) and 21 (South Mozambique Channel) during MAD-Ridge. White dotted lines represent the trawl path as determined from Scanmar depth sensor. The seamount summit is denoted by the black polygon and labelled accordingly. The 38 kHz, 70 kHz and 120 kHz frequencies were given red, green and blue colour codes respectively. Corresponding frequency diagrams of the species count and frequency responses for trawls #14, 15, 16 and 21 are given. Broad categories are coloured orange (crustaceans), yellow (fishes), blue (gelatinous organisms), and violet (cephalopods).

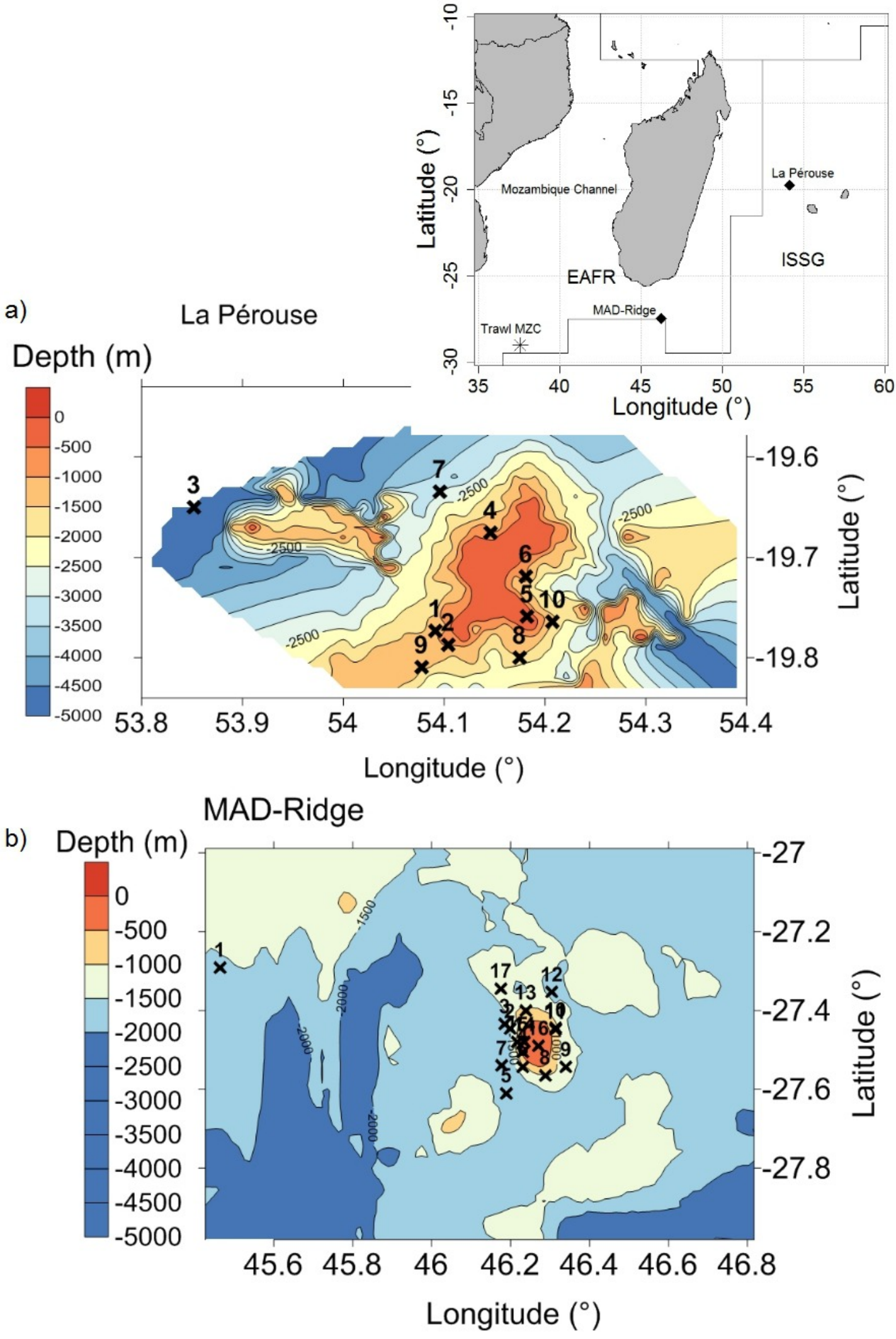
Mozambique Channel
La Pérouse
ISSG
EAFR
MAD-Ridge
Trawl MZC
Latitude (°)
Longitude (°)
a)
La Pérouse
Depth (m)
0
-500
-1000
-1500
-2000
-2500
-3000
-3500
-4000
-4500
-5000
-19.6
-19.7
-19.8
53.8
53.9
54
54.1
54.2
54.3
54.4
b)
MAD-Ridge
-27
-27.2
-27.4
-27.6
-27.8
45.6
45.8
46
46.2
46.4
46.6
46.8

Figure 1

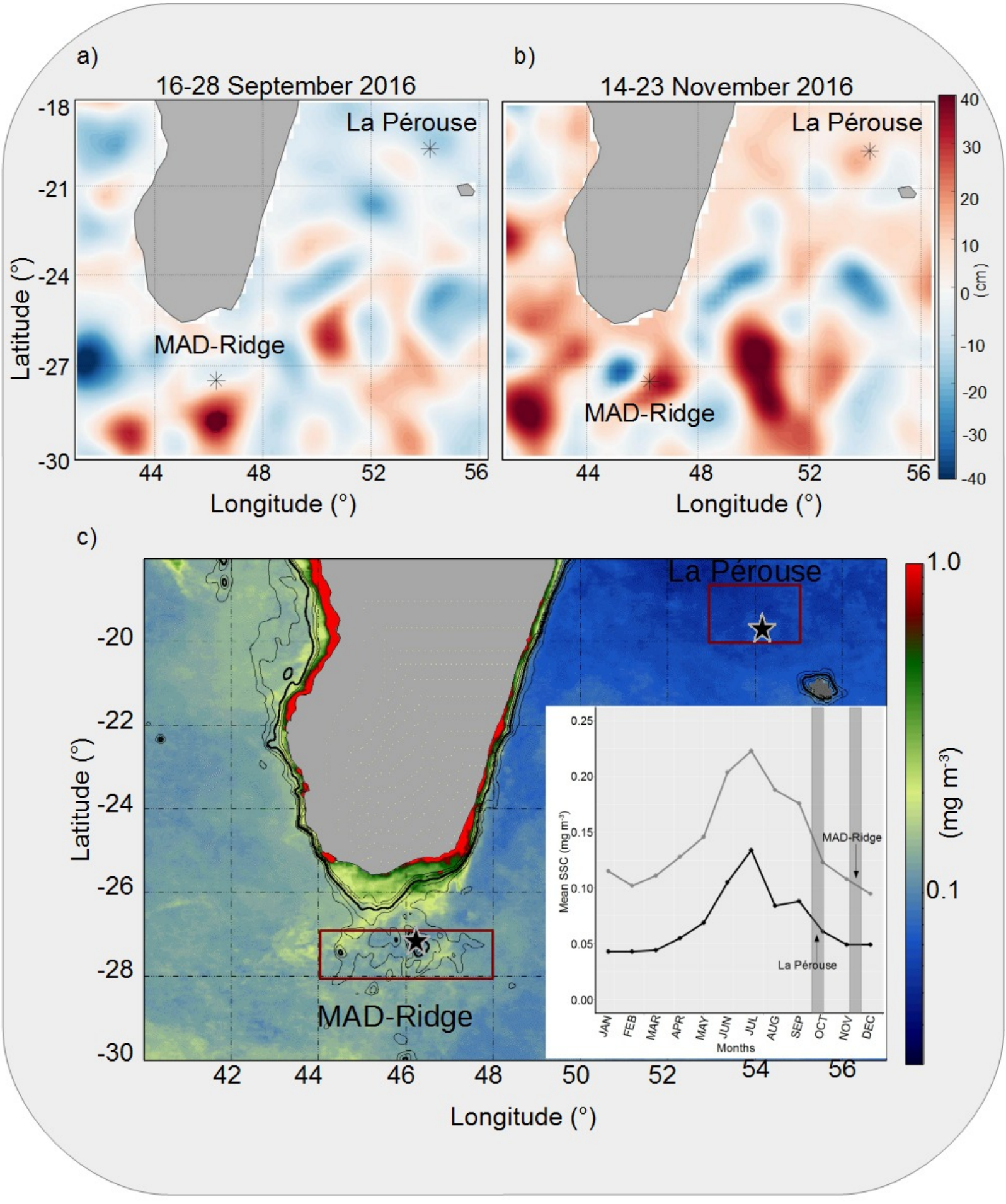
a)
16-28 September 2016
La Pérouse
MAD-Ridge
Latitude (°)
Longitude (°)
b)
14-23 November 2016
La Pérouse
MAD-Ridge
Longitude (°)
(cm)
c)
La Pérouse
MAD-Ridge
Latitude (°)
Longitude (°)
Mean SSC (mg m-3)
Months
JAN
FEB
MAR
APR
MAY
JUN
JUL
AUG
SEP
OCT
NOV
DEC
(mg m-3)

Figure 2

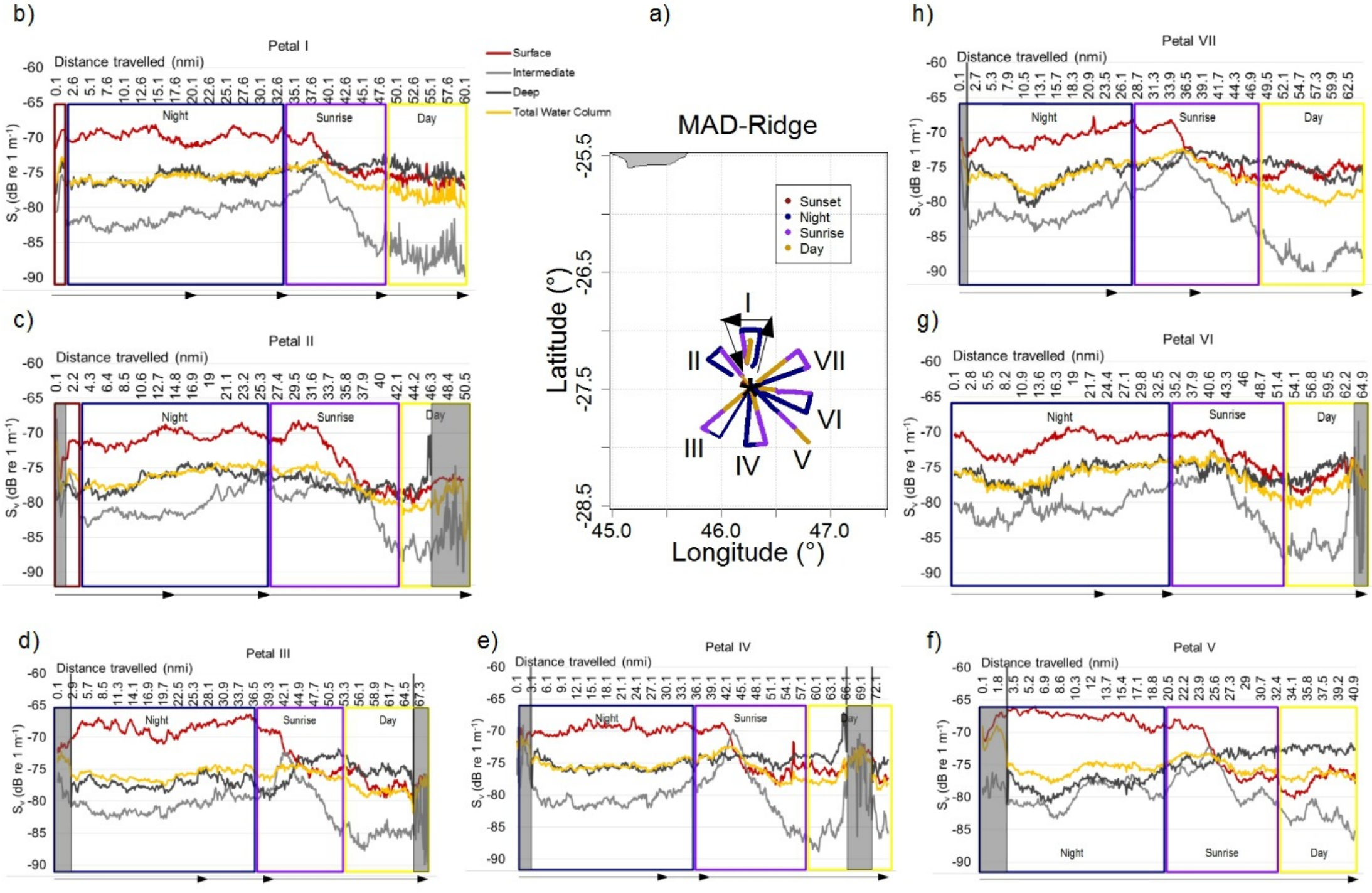
a)
MAD-Ridge
Surface
Intermediate
Deep
Total Water Column
Sunset
Night
Sunrise
Day
I
II
III
IV
V
VI
VII
Latitude (°)
Longitude (°)
-25.5
-26.5
-27.5
-28.5
45.0
46.0
47.0
b)
Petal I
c)
Petal II
d)
Petal III
e)
Petal IV
f)
Petal V
g)
Petal VI
h)
Petal VII
Distance travelled (nmi)
Night
Sunrise
Day
S_v (dB re 1 m^{-1})

Figure 3

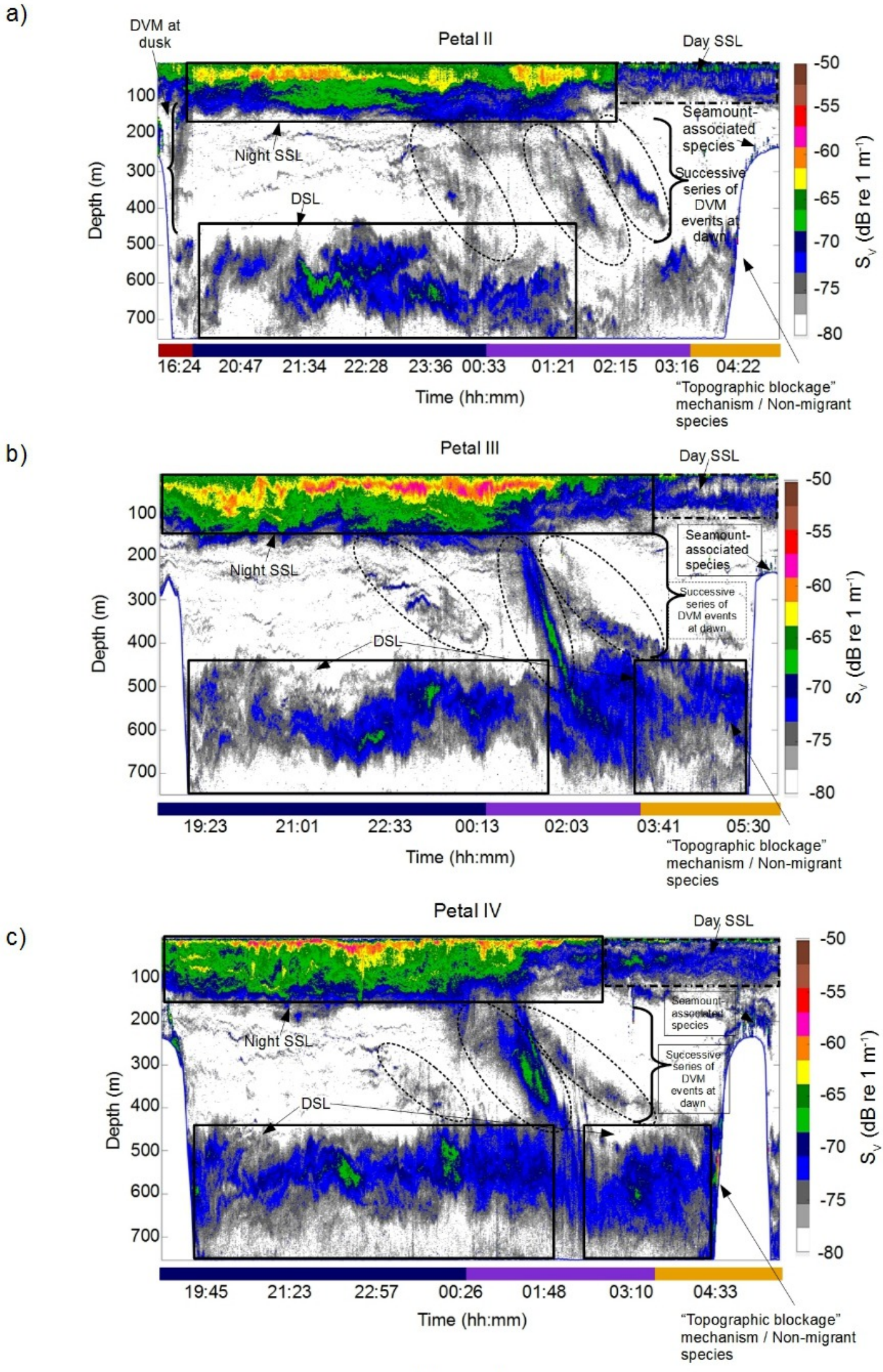
a)
Petal II
DVM at dusk
Day SSL
Night SSL
Seamount-associated species
Successive series of DVM events at dawn
DSL
Depth (m)
100
200
300
400
500
600
700
-50
-55
-60
-65
-70
-75
-80
S_v (dB re 1 m^{-1})
16:24
20:47
21:34
22:28
23:36
00:33
01:21
02:15
03:16
04:22
Time (hh:mm)
"Topographic blockage" mechanism / Non-migrant species
b)
Petal III
Day SSL
Night SSL
Seamount-associated species
Successive series of DVM events at dawn
DSL
Depth (m)
19:23
21:01
22:33
00:13
02:03
03:41
05:30
Time (hh:mm)
"Topographic blockage" mechanism / Non-migrant species
c)
Petal IV
Day SSL
Night SSL
Seamount-associated species
Successive series of DVM events at dawn
DSL
Depth (m)
19:45
21:23
22:57
00:26
01:48
03:10
04:33
Time (hh:mm)
"Topographic blockage" mechanism / Non-migrant species

Figure 4

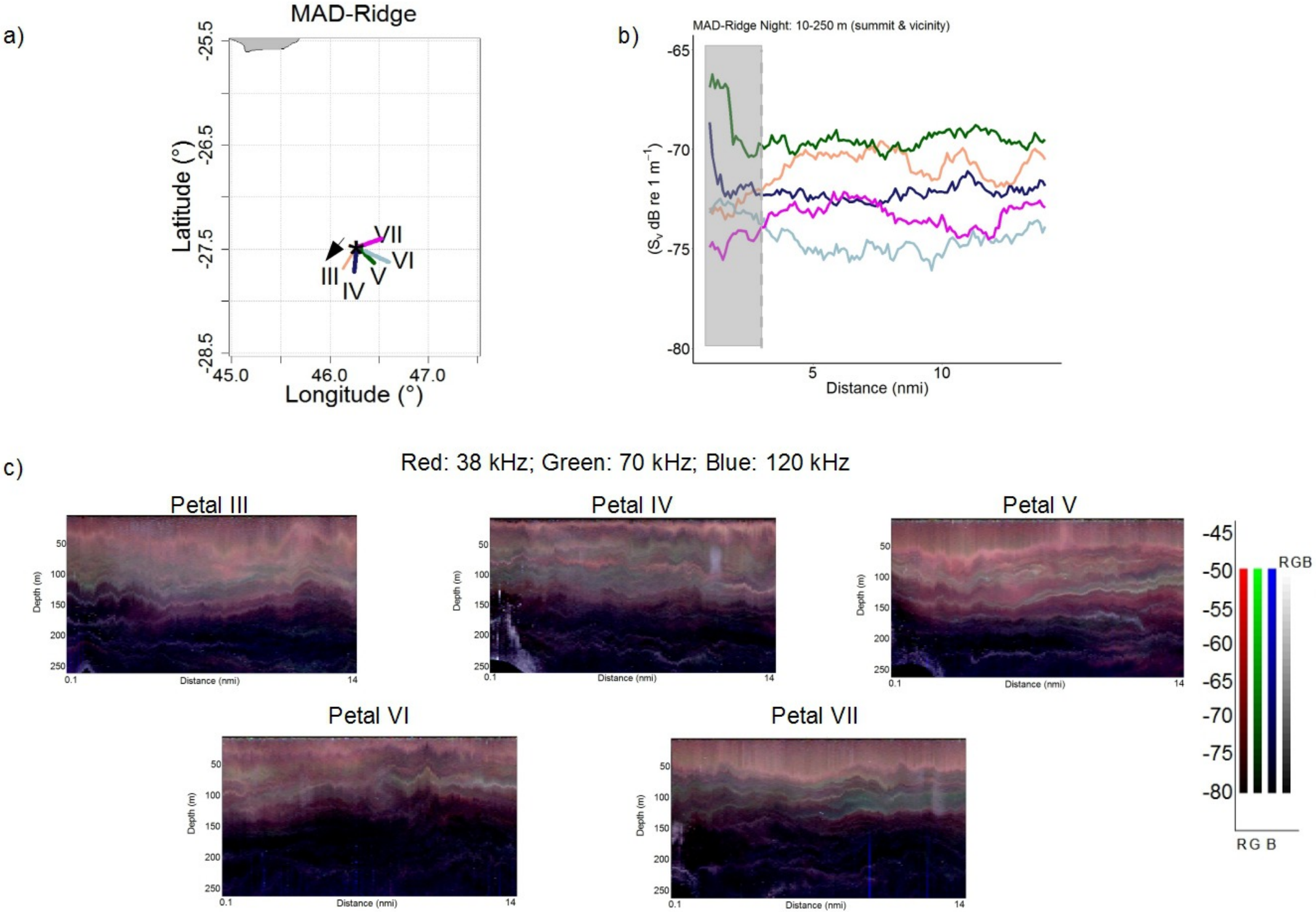
a)
MAD-Ridge
Latitude (°)
-25.5
-26.5
-27.5
-28.5
45.0
46.0
47.0
Longitude (°)
III
IV
V
VI
VII
b)
MAD-Ridge Night: 10-250 m (summit & vicinity)
(S_v dB re 1 m^-1)
-65
-70
-75
-80
5
10
Distance (nmi)
c)
Red: 38 kHz; Green: 70 kHz; Blue: 120 kHz
Petal III
Petal IV
Petal V
Petal VI
Petal VII
Depth (m)
50
100
150
200
250
0.1
Distance (nmi)
14
-45
-50
-55
-60
-65
-70
-75
-80
RGB
RG B

Figure 5

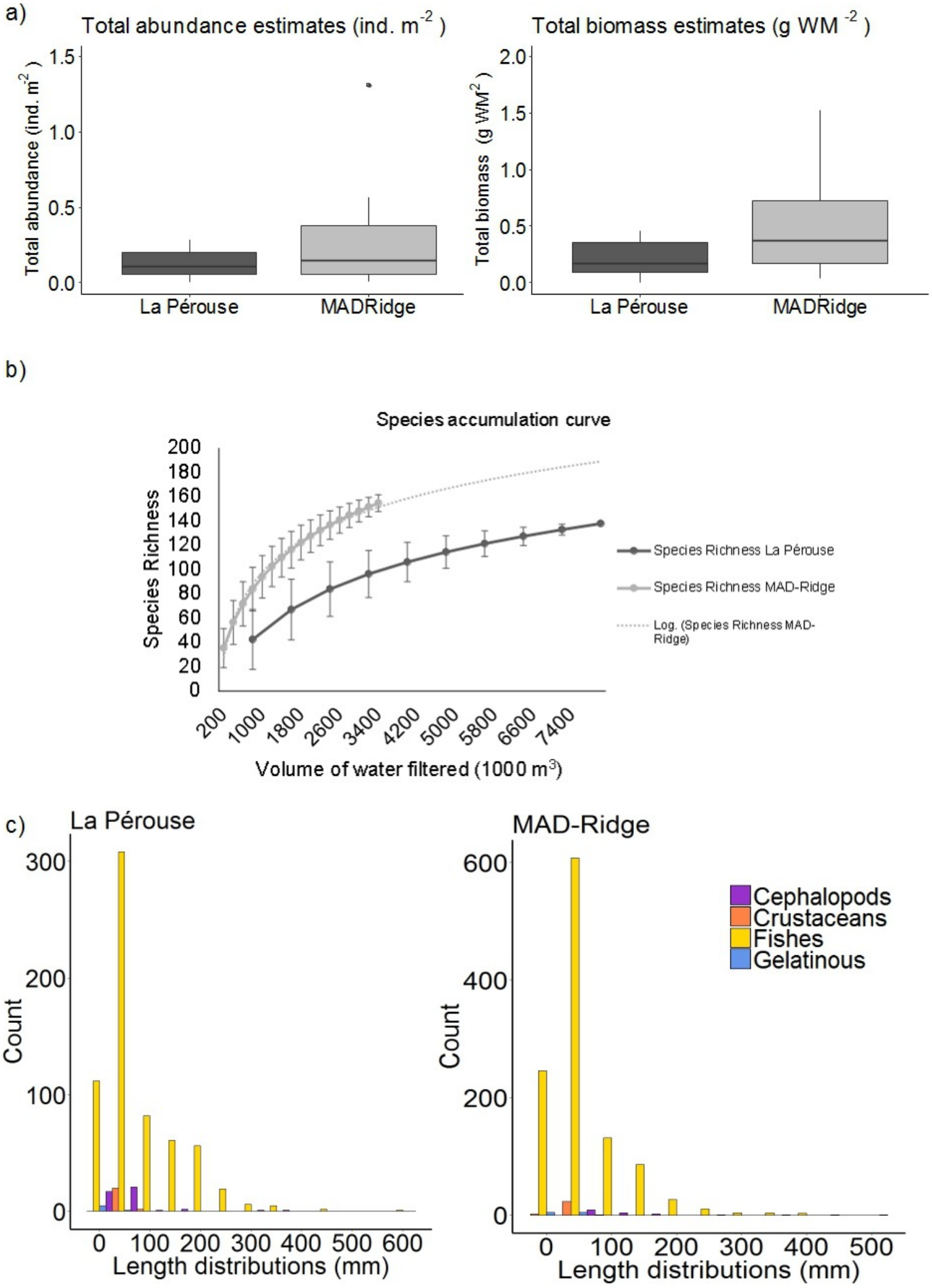
a)
Total abundance estimates (ind. m-2)
Total abundance (ind. m-2)
1.5
1.0
0.5
0.0
La Pérouse
MADRidge
Total biomass estimates (g WM -2)
Total biomass (g WM2)
2.0
1.5
1.0
0.5
0.0
La Pérouse
MADRidge
b)
Species accumulation curve
Species Richness
200
180
160
140
120
100
80
60
40
20
0
200
1000
1800
2600
3400
4200
5000
5800
6600
7400
Volume of water filtered (1000 m3)
Species Richness La Pérouse
Species Richness MAD-Ridge
Log. (Species Richness MAD-Ridge)
c)
La Pérouse
Count
300
200
100
0
0 100 200 300 400 500 600
Length distributions (mm)
MAD-Ridge
Count
600
400
200
0
0 100 200 300 400 500
Length distributions (mm)
Cephalopods
Crustaceans
Fishes
Gelatinous

Figure 6

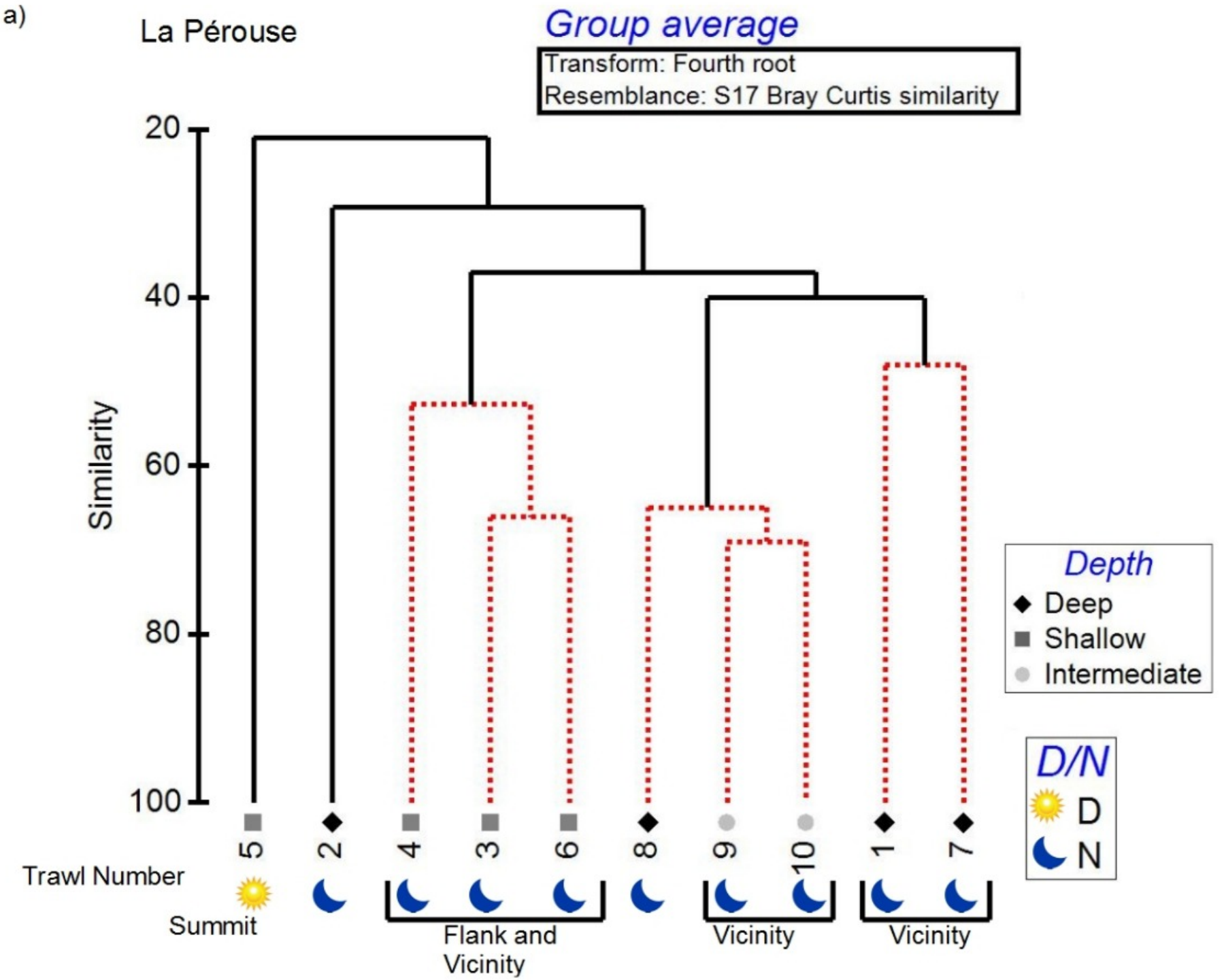
a)
La Pérouse
Group average
Transform: Fourth root
Resemblance: S17 Bray Curtis similarity
Similarity
20
40
60
80
100
Depth
Deep
Shallow
Intermediate
D/N
D
N
Trawl Number
5
2
4
3
6
8
9
10
1
7
Summit
Flank and Vicinity
Vicinity
Vicinity

Figure 7

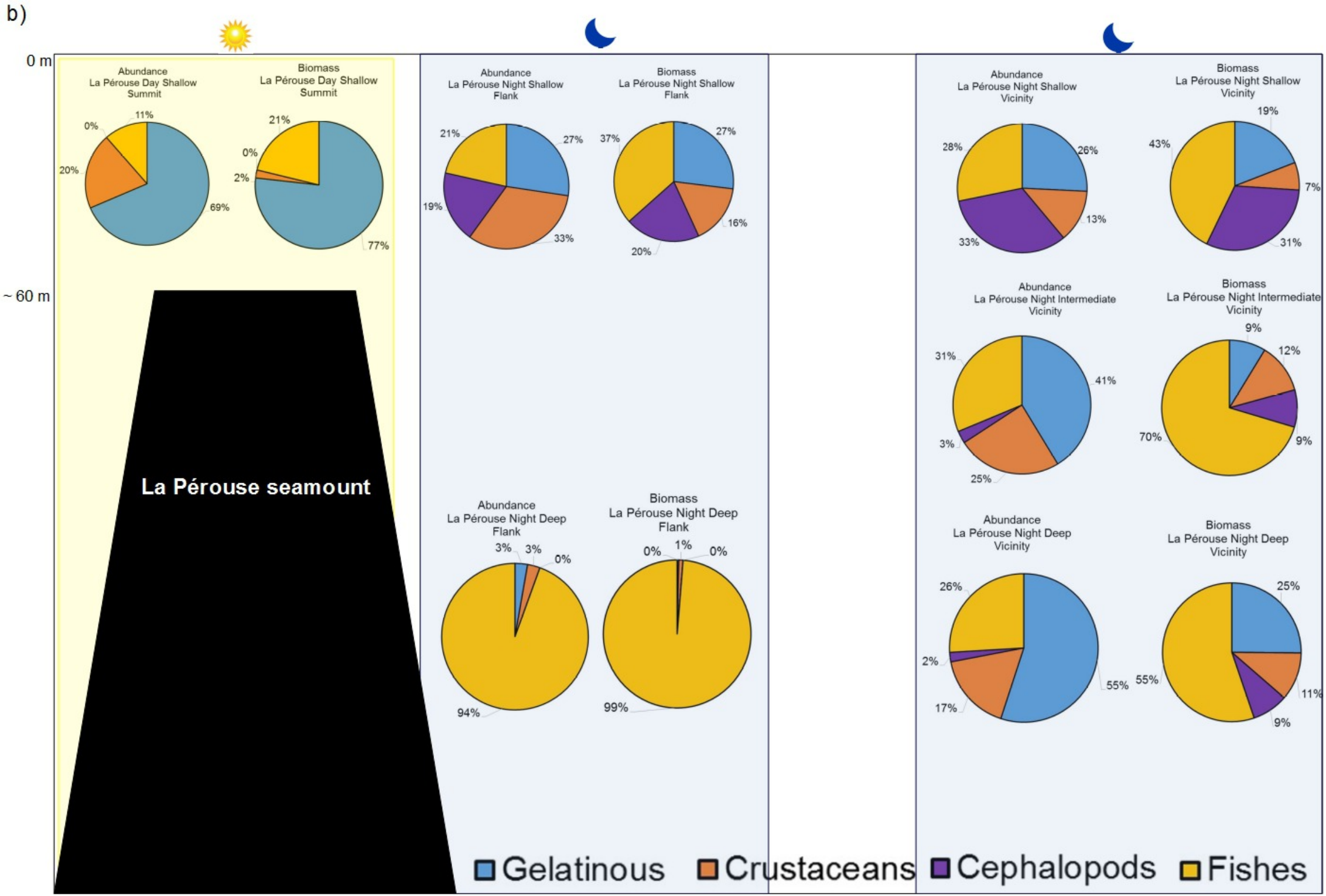
b)
0 m
~ 60 m
La Pérouse seamount
Abundance
La Pérouse Day Shallow
Summit
11%
0%
20%
69%
Biomass
La Pérouse Day Shallow
Summit
21%
0%
2%
77%
Abundance
La Pérouse Night Shallow
Flank
21%
27%
19%
33%
Biomass
La Pérouse Night Shallow
Flank
37%
27%
16%
20%
Abundance
La Pérouse Night Deep
Flank
3%
3%
0%
94%
Biomass
La Pérouse Night Deep
Flank
0%
1%
0%
99%
Abundance
La Pérouse Night Shallow
Vicinity
28%
26%
13%
33%
Biomass
La Pérouse Night Shallow
Vicinity
19%
43%
7%
31%
Abundance
La Pérouse Night Intermediate
Vicinity
31%
41%
3%
25%
Biomass
La Pérouse Night Intermediate
Vicinity
9%
12%
70%
9%
Abundance
La Pérouse Night Deep
Vicinity
26%
2%
55%
17%
Biomass
La Pérouse Night Deep
Vicinity
25%
55%
11%
9%
Gelatinous
Crustaceans
Cephalopods
Fishes

Figure 7

c) Deep dwelling organisms at La Pérouse

Pasiphaea sp. (crustacean)

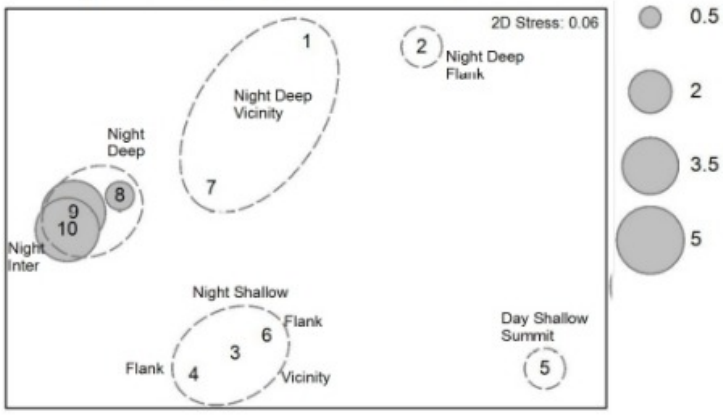

Argyropelecus aculeatus (fish)

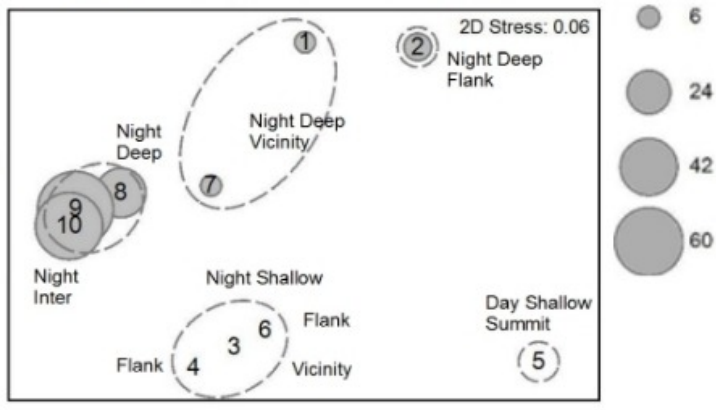

d) Seamount flank associated fish species at La Pérouse

Diaphus suborbitalis

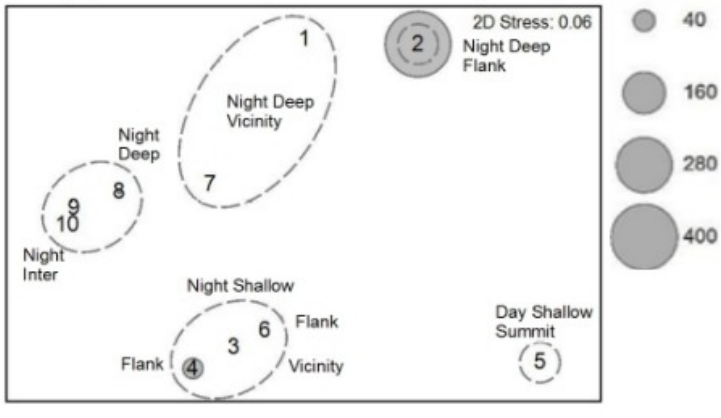

Argyripnus hulleyi

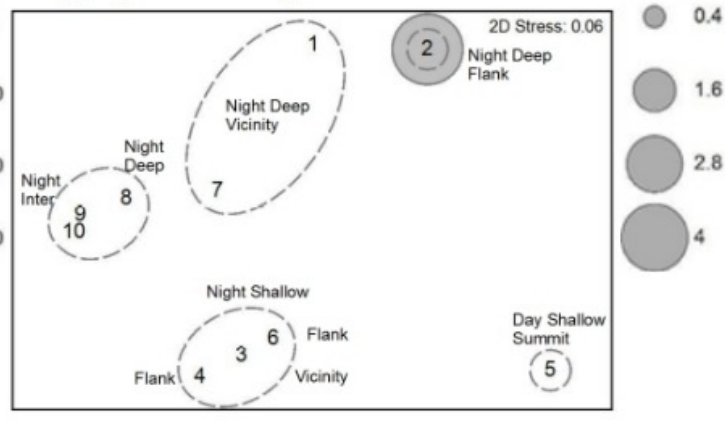

Figure 7

a)

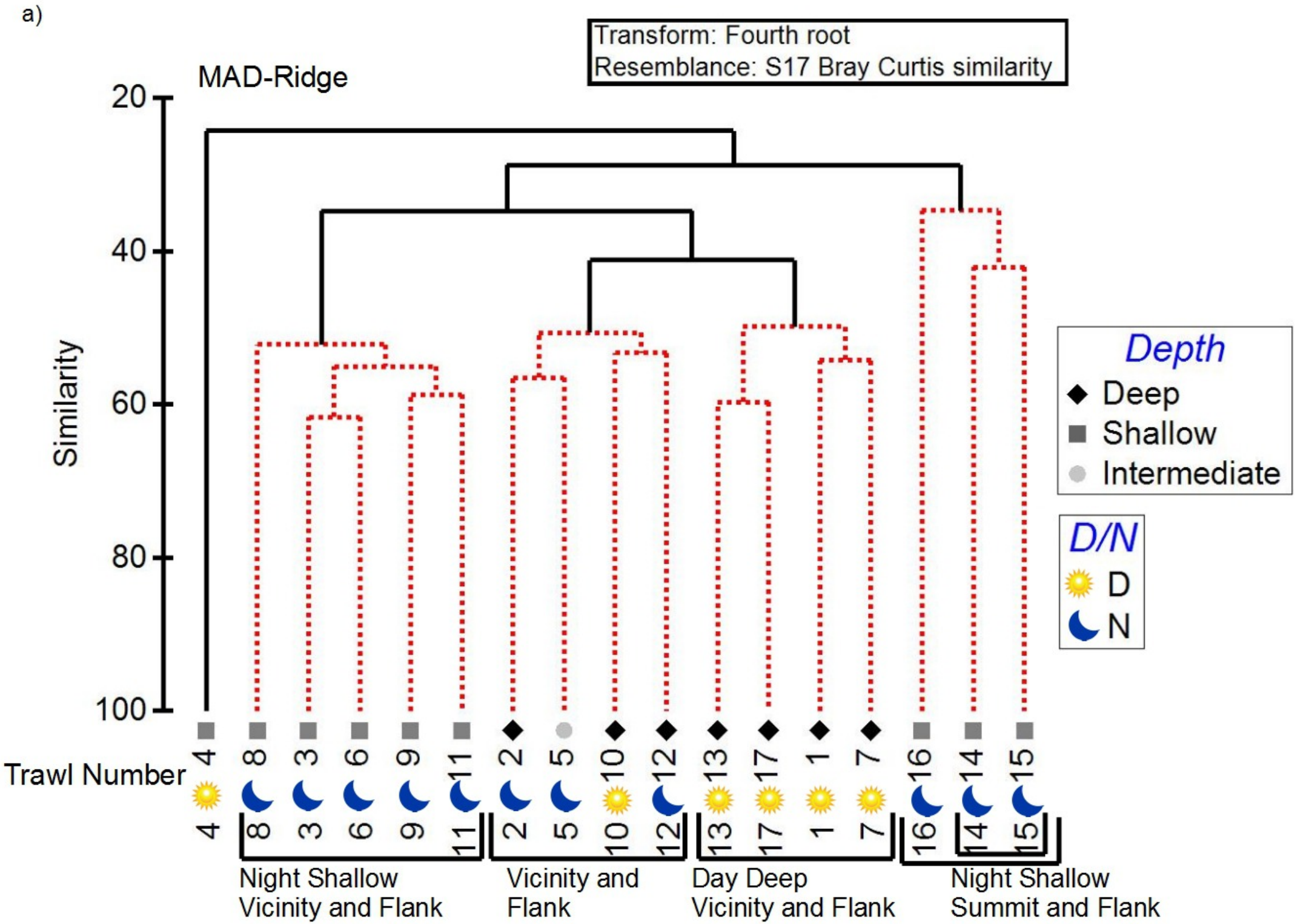
Transform: Fourth root
Resemblance: S17 Bray Curtis similarity
MAD-Ridge
Similarity
20
40
60
80
100
Depth
Deep
Shallow
Intermediate
D/N
D
N
Trawl Number
4 8 3 6 9 11 2 5 10 12 13 17 1 7 16 14 15
4 8 3 6 9 11 2 5 10 12 13 17 1 7 16 14 15
Night Shallow
Vicinity and Flank
Vicinity and
Flank
Day Deep
Vicinity and Flank
Night Shallow
Summit and Flank

Figure 8

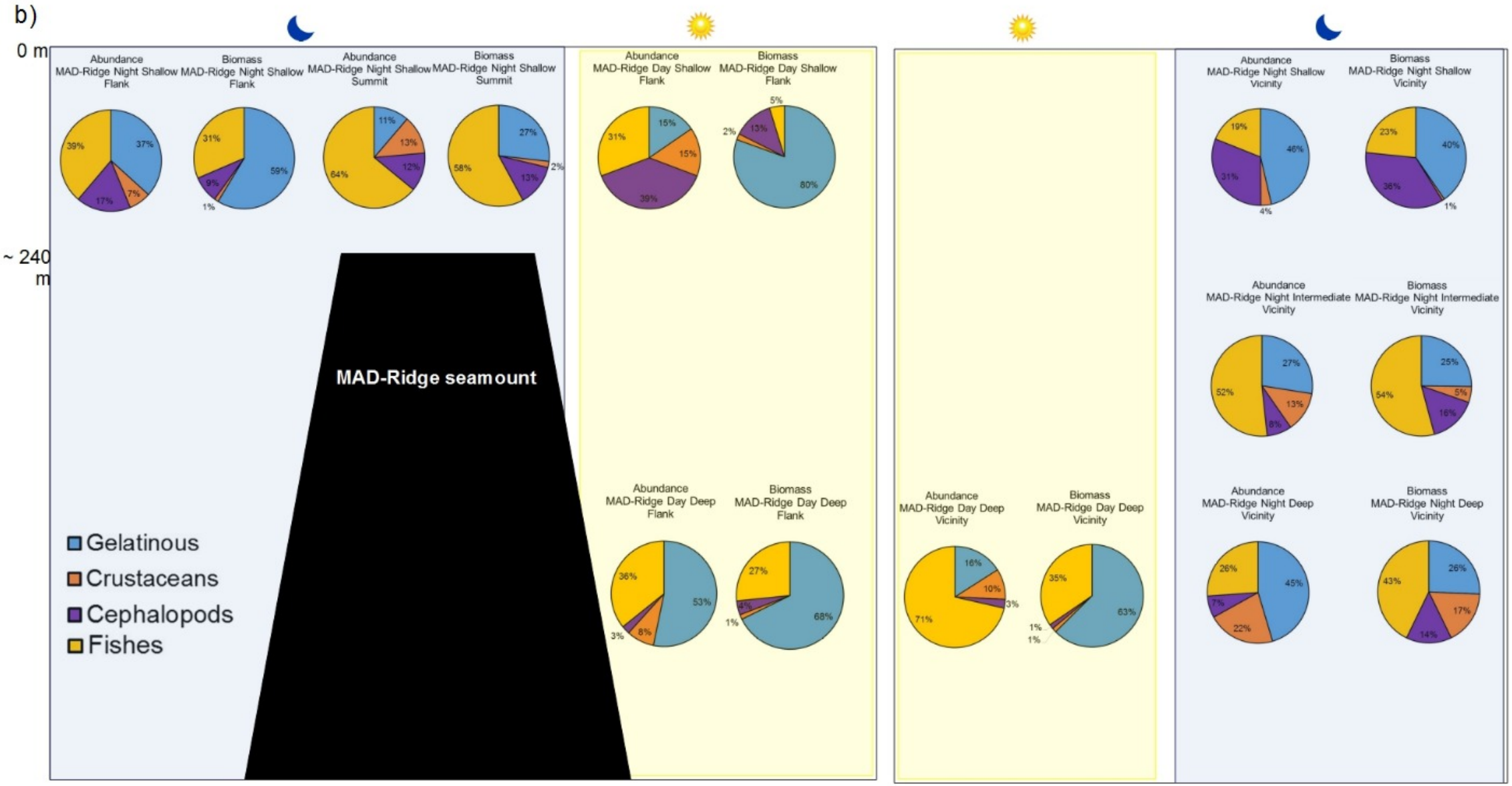
b)
0 m
~ 240 m
Abundance MAD-Ridge Night Shallow Flank
Biomass MAD-Ridge Night Shallow Flank
Abundance MAD-Ridge Night Shallow Summit
Biomass MAD-Ridge Night Shallow Summit
Abundance MAD-Ridge Day Shallow Flank
Biomass MAD-Ridge Day Shallow Flank
Abundance MAD-Ridge Night Shallow Vicinity
Biomass MAD-Ridge Night Shallow Vicinity
Abundance MAD-Ridge Night Intermediate Vicinity
Biomass MAD-Ridge Night Intermediate Vicinity
Abundance MAD-Ridge Day Deep Flank
Biomass MAD-Ridge Day Deep Flank
Abundance MAD-Ridge Day Deep Vicinity
Biomass MAD-Ridge Day Deep Vicinity
Abundance MAD-Ridge Night Deep Vicinity
Biomass MAD-Ridge Night Deep Vicinity
MAD-Ridge seamount
Gelatinous
Crustaceans
Cephalopods
Fishes

Figure 8

c) Shallow-dwelling and vertical migratory fish at MAD-Ridge

Acanthuridae sp.

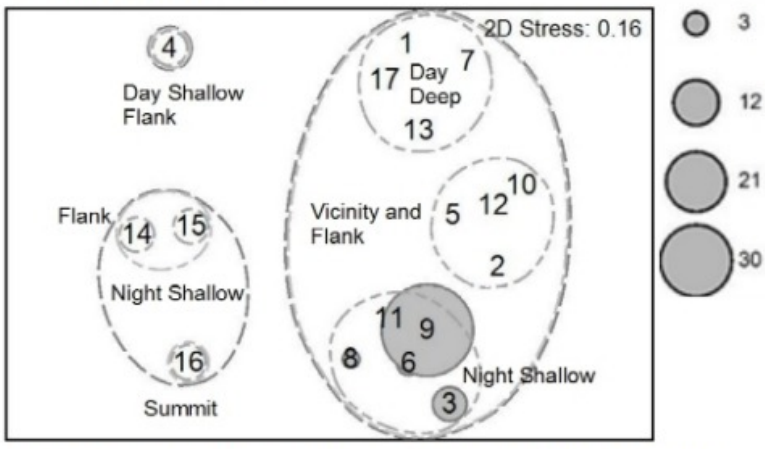

Ceratoscopelus warmingii

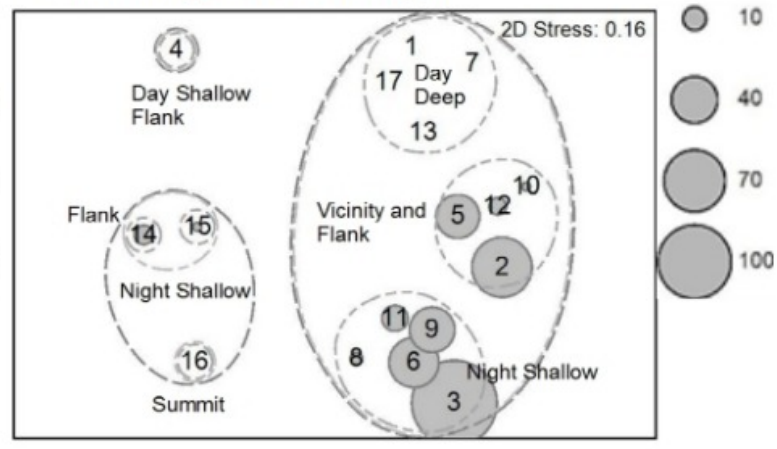

d) Deep-dwelling fish species at MAD-Ridge

Cyclothone sp.

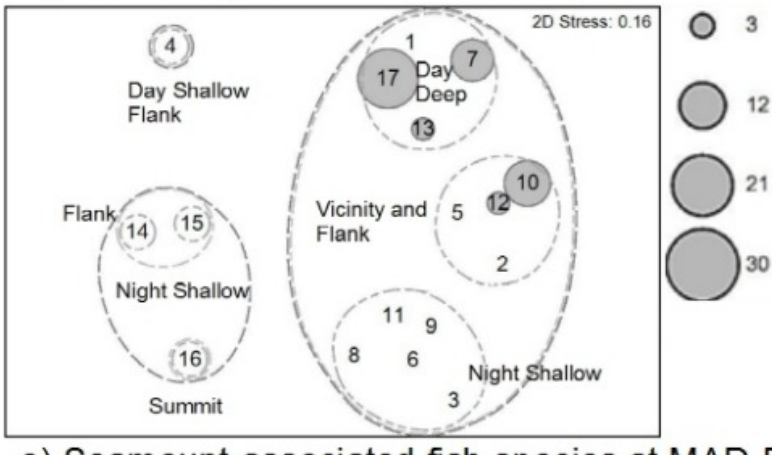

Argyropelecus aculeatus

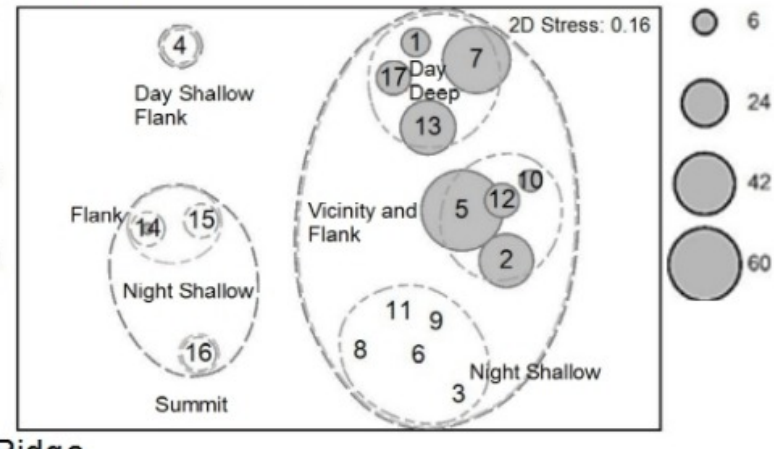

e) Seamount-associated fish species at MAD-Ridge

Diaphus suborbitalis

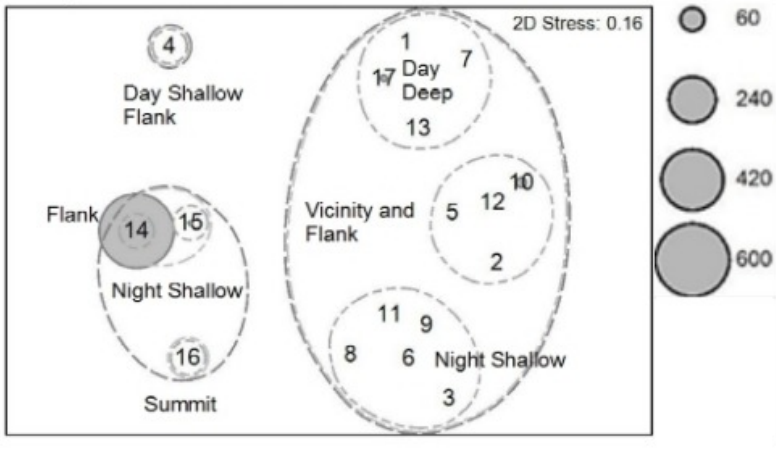

Neoscopelus macrolepidotus

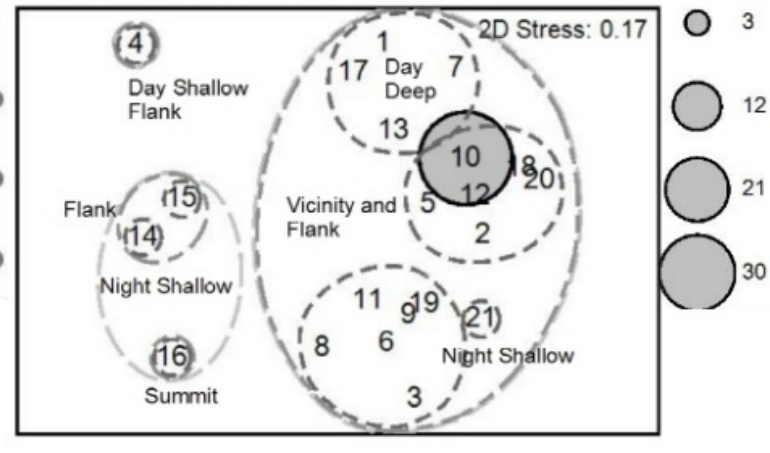

Benthosema fibulatum

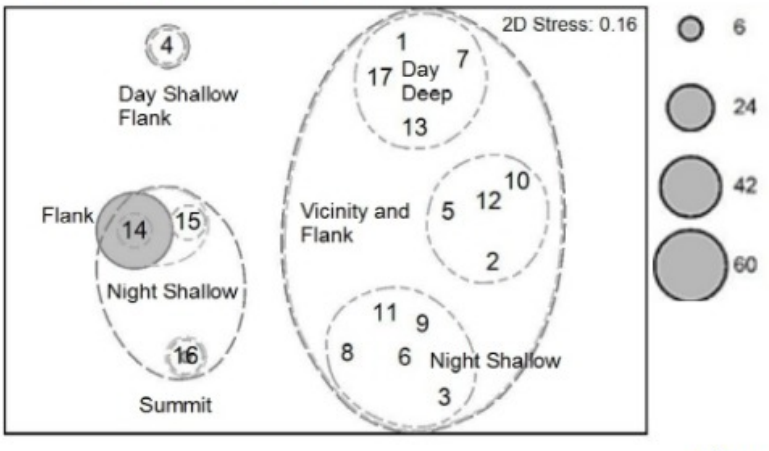

Cookeolus japonicus

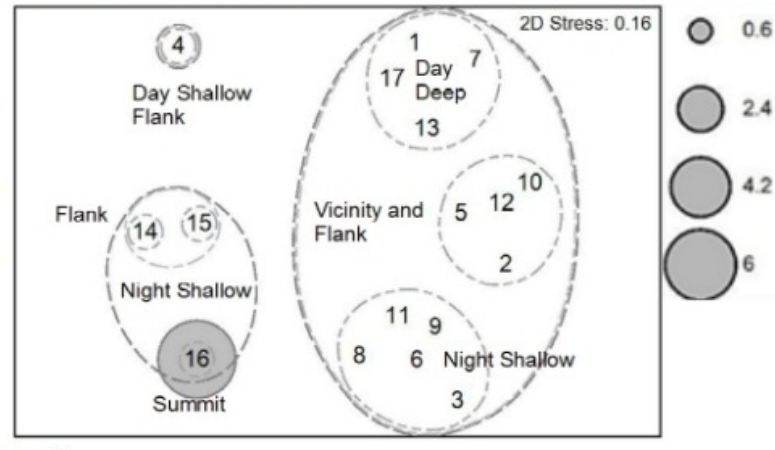

Figure 8

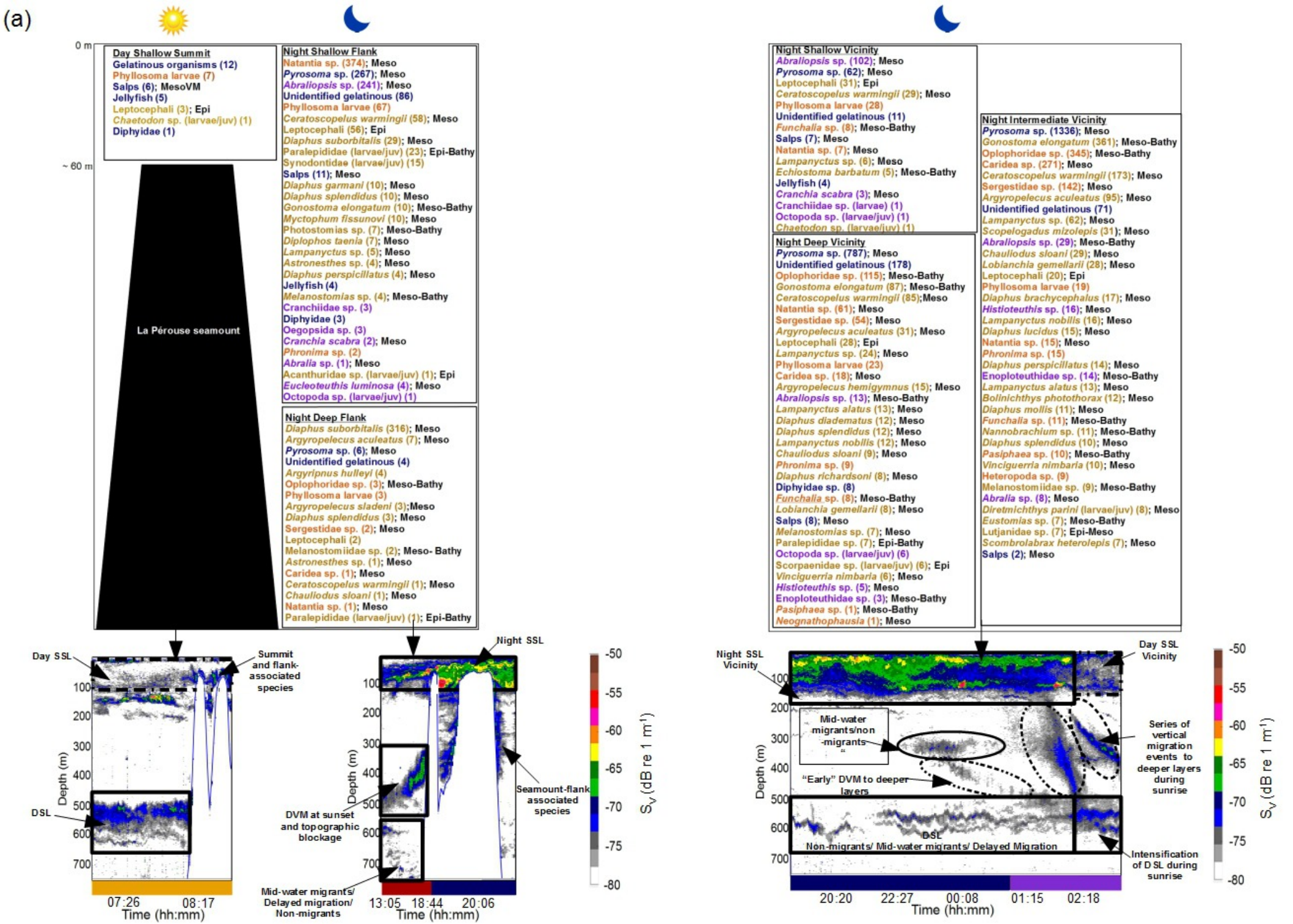
(a)
0 m
~ 60 m
La Pérouse seamount
Day Shallow Summit
Gelatinous organisms (12)
Phyllosoma larvae (7)
Salps (6); MesoVM
Jellyfish (5)
Leptocephali (3); Epi
Chaetodon sp. (larvae/juv) (1)
Diphyidae (1)
Night Shallow Flank
Natantia sp. (374); Meso
Pyrosoma sp. (267); Meso
Abraliopsis sp. (241); Meso
Unidentified gelatinous (86)
Phyllosoma larvae (67)
Ceratoscopelus warmingii (58); Meso
Leptocephali (56); Epi
Diaphus suborbitalis (29); Meso
Paralepididae (larvae/juv) (23); Epi-Bathy
Synodontidae (larvae/juv) (15)
Salps (11); Meso
Diaphus garmani (10); Meso
Diaphus splendidus (10); Meso
Gonostoma elongatum (10); Meso-Bathy
Myctophum fissunovi (10); Meso
Photostomias sp. (7); Meso-Bathy
Diplophos taenia (7); Meso
Lampanyctus sp. (5); Meso
Astronesthes sp. (4); Meso
Diaphus perspicillatus (4); Meso
Jellyfish (4)
Melanostomias sp. (4); Meso-Bathy
Cranchiidae sp. (3)
Diphyidae (3)
Oegopsida sp. (3)
Cranchia scabra (2); Meso
Phronima sp. (2)
Abralia sp. (1); Meso
Acanthuridae sp. (larvae/juv) (1); Epi
Eucleoteuthis luminosa (4); Meso
Octopoda sp. (larvae/juv) (1)
Night Deep Flank
Diaphus suborbitalis (316); Meso
Argyropelecus aculeatus (7); Meso
Pyrosoma sp. (6); Meso
Unidentified gelatinous (4)
Argyripnus hulleyi (4)
Oplophoridae sp. (3); Meso-Bathy
Phyllosoma larvae (3)
Argyropelecus sladeni (3);Meso
Diaphus splendidus (3); Meso
Sergestidae sp. (2); Meso
Leptocephali (2)
Melanostomiidae sp. (2); Meso- Bathy
Astronesthes sp. (1); Meso
Caridea sp. (1); Meso
Ceratoscopelus warmingii (1); Meso
Chauliodus sloani (1); Meso
Natantia sp. (1); Meso
Paralepididae (larvae/juv) (1); Epi-Bathy
Night Shallow Vicinity
Abraliopsis sp. (102); Meso
Pyrosoma sp. (62); Meso
Leptocephali (31); Epi
Ceratoscopelus warmingii (29); Meso
Phyllosoma larvae (28)
Unidentified gelatinous (11)
Funchalia sp. (8); Meso-Bathy
Salps (7); Meso
Natantia sp. (7); Meso
Lampanyctus sp. (6); Meso
Echiostoma barbatum (5); Meso-Bathy
Jellyfish (4)
Cranchia scabra (3); Meso
Cranchiidae sp. (larvae) (1)
Octopoda sp. (larvae/juv) (1)
Chaetodon sp. (larvae/juv) (1)
Night Deep Vicinity
Pyrosoma sp. (787); Meso
Unidentified gelatinous (178)
Oplophoridae sp. (115); Meso-Bathy
Gonostoma elongatum (87); Meso-Bathy
Ceratoscopelus warmingii (85);Meso
Natantia sp. (61); Meso
Sergestidae sp. (54); Meso
Argyropelecus aculeatus (31); Meso
Leptocephali (28); Epi
Lampanyctus sp. (24); Meso
Phyllosoma larvae (23)
Caridea sp. (18); Meso
Argyropelecus hemigymnus (15); Meso
Abraliopsis sp. (13); Meso-Bathy
Lampanyctus alatus (13); Meso
Diaphus dilodematus (12); Meso
Diaphus splendidus (12); Meso
Lampanyctus nobilis (12); Meso
Chauliodus sloani (9); Meso
Phronima sp. (9)
Diaphus richardsoni (8); Meso
Diphyidae sp. (8)
Funchalia sp. (8); Meso-Bathy
Lobianchia gemellarii (8); Meso
Salps (8); Meso
Melanostomias sp. (7); Meso
Paralepididae sp. (7); Epi-Bathy
Octopoda sp. (larvae/juv) (6)
Scorpaenidae sp. (larvae/juv) (6); Epi
Vinciguerria nimbaria (6); Meso
Histioteuthis sp. (5); Meso
Enoploteuthidae sp. (3); Meso-Bathy
Pasiphaea sp. (1); Meso-Bathy
Neognathophausia (1); Meso
Night Intermediate Vicinity
Pyrosoma sp. (1336); Meso
Gonostoma elongatum (361); Meso-Bathy
Oplophoridae sp. (345); Meso-Bathy
Caridea sp. (271); Meso
Ceratoscopelus warmingii (173); Meso
Sergestidae sp. (142); Meso
Argyropelecus aculeatus (95); Meso
Unidentified gelatinous (71)
Lampanyctus sp. (62); Meso
Scopelogadus mizolepis (31); Meso
Abraliopsis sp. (29); Meso-Bathy
Chauliodus sloani (29); Meso
Lobianchia gemellarii (28); Meso
Leptocephali (20); Epi
Phyllosoma larvae (19)
Diaphus brachycephalus (17); Meso
Histioteuthis sp. (16); Meso
Lampanyctus nobilis (16); Meso
Diaphus lucidus (15); Meso
Natantia sp. (15); Meso
Phronima sp. (15)
Diaphus perspicillatus (14); Meso
Enoploteuthidae sp. (14); Meso-Bathy
Lampanyctus alatus (13); Meso
Bolinichthys photothorax (12); Meso
Diaphus mollis (11); Meso
Funchalia sp. (11); Meso-Bathy
Nannobrachium sp. (11); Meso-Bathy
Diaphus splendidus (10); Meso
Pasiphaea sp. (10); Meso-Bathy
Vinciguerria nimbaria (10); Meso
Heteropoda sp. (9)
Melanostomiidae sp. (9); Meso-Bathy
Abralia sp. (8); Meso
Diretmichthys parini (larvae/juv) (8); Meso
Eustomias sp. (7); Meso-Bathy
Lutjanidae sp. (7); Epi-Meso
Scombrolabrax heterolepis (7); Meso
Salps (2); Meso
Day SSL
Summit and flank-associated species
DSL
Depth (m)
Time (hh:mm)
07:26
08:17
Night SSL
DVM at sunset and topographic blockage
Seamount-flank associated species
Mid-water migrants/ Delayed migration/ Non-migrants
13:05
18:44
20:06
Night SSL Vicinity
Day SSL Vicinity
Mid-water migrants/non -migrants
Series of vertical migration events to deeper layers during sunrise
"Early" DVM to deeper layers
DSL
Non-migrants/ Mid-water migrants/ Delayed Migration
Intensification of DSL during sunrise
20:20
22:27
00:08
01:15
02:18
S_v (dB re 1 m^{-1})
-50
-55
-60
-65
-70
-75
-80

Figure 9

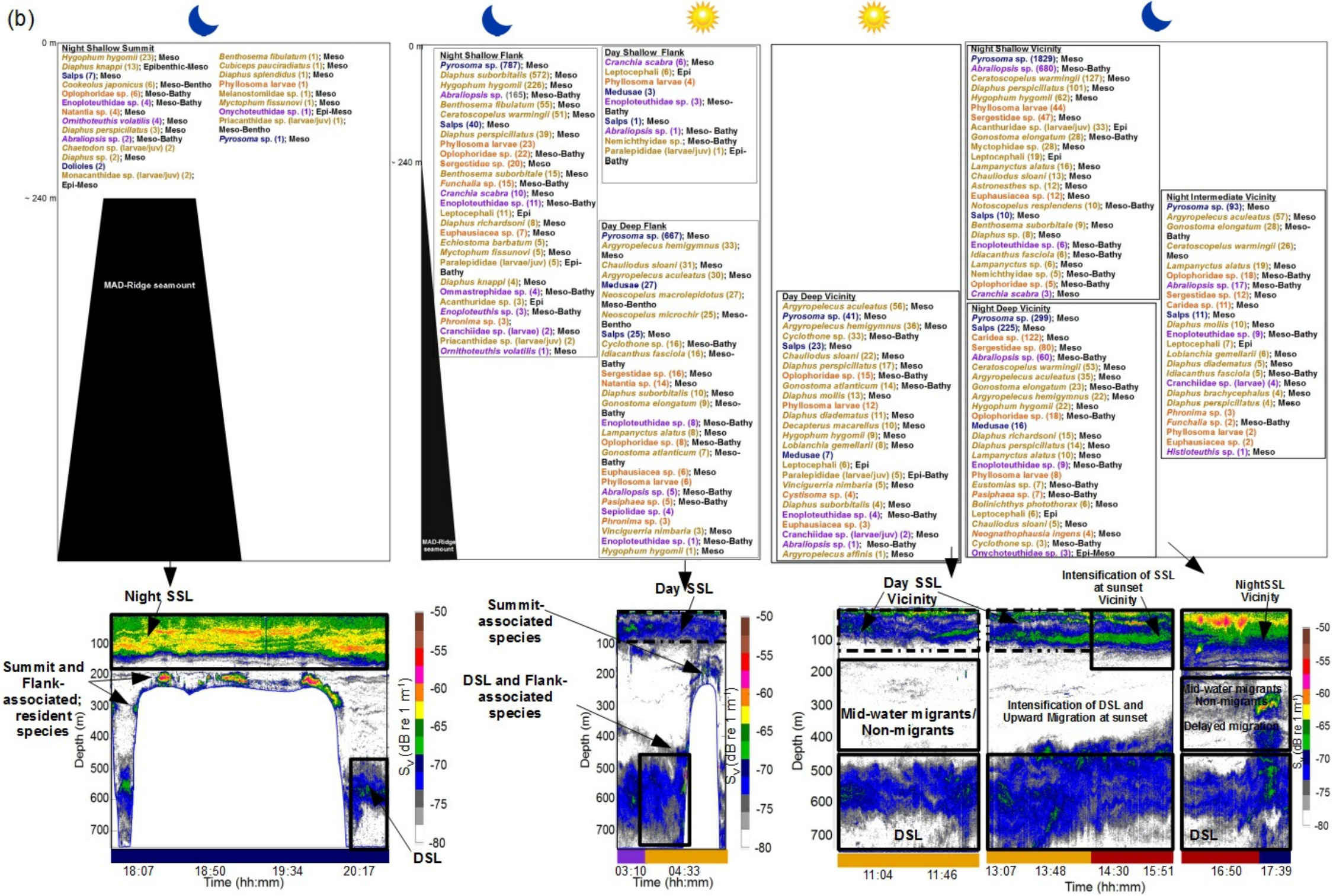
(b)
0 m
~ 240 m
Night Shallow Summit
Hygophum hygomii (23); Meso
Diaphus knappi (13); Epibenthic-Meso
Salps (7); Meso
Cookeolus japonicus (6); Meso-Bentho
Oplophoridae sp. (6); Meso-Bathy
Enoploteuthidae sp. (4); Meso-Bathy
Natantia sp. (4); Meso
Ornithoteuthis volatilis (4); Meso
Diaphus perspicillatus (3); Meso
Abraliopsis sp. (2); Meso-Bathy
Chaetodon sp. (larvae/juv) (2)
Diaphus sp. (2); Meso
Dolioles (2)
Monacanthidae sp. (larvae/juv) (2); Epi-Meso
Benthosema fibulatum (1); Meso
Cubiceps pauciradiatus (1); Meso
Diaphus splendidus (1); Meso
Phyllosoma larvae (1)
Melanostomiidae sp. (1); Meso
Myctophum fissunovi (1); Meso
Onychoteuthidae sp. (1); Epi-Meso
Priacanthidae sp. (larvae/juv) (1); Meso-Bentho
Pyrosoma sp. (1); Meso
MAD-Ridge seamount
Night Shallow Flank
Pyrosoma sp. (787); Meso
Diaphus suborbitalis (572); Meso
Hygophum hygomii (226); Meso
Abraliopsis sp. (165); Meso-Bathy
Benthosema fibulatum (55); Meso
Ceratoscopelus warmingii (51); Meso
Salps (40); Meso
Diaphus perspicillatus (39); Meso
Phyllosoma larvae (23)
Oplophoridae sp. (22); Meso-Bathy
Sergestidae sp. (20); Meso
Benthosema suborbitale (15); Meso
Funchalia sp. (15); Meso-Bathy
Cranchia scabra (10); Meso
Enoploteuthidae sp. (11); Meso-Bathy
Leptocephali (11); Epi
Diaphus richardsoni (8); Meso
Euphausiacea sp. (7); Meso
Echiostoma barbatum (5);
Myctophum fissunovi (5); Meso
Paralepididae (larvae/juv) (5); Epi-Bathy
Diaphus knappi (4); Meso
Ommastrephidae sp. (4); Meso-Bathy
Acanthuridae sp. (3); Epi
Enoploteuthis sp. (3); Meso-Bathy
Phronima sp. (3);
Cranchiidae sp. (larvae) (2); Meso
Priacanthidae sp. (larvae/juv) (2)
Ornithoteuthis volatilis (1); Meso
Day Shallow Flank
Cranchia scabra (6); Meso
Leptocephali (6); Epi
Phyllosoma larvae (4)
Medusae (3)
Enoploteuthidae sp. (3); Meso-Bathy
Salps (1); Meso
Abraliopsis sp. (1); Meso- Bathy
Nemichthyidae sp.; Meso-Bathy
Paralepididae (larvae/juv) (1); Epi-Bathy
Day Deep Flank
Pyrosoma sp. (667); Meso
Argyropelecus hemigymnus (33); Meso
Chauliodus sloani (31); Meso
Argyropelecus aculeatus (30); Meso
Medusae (27)
Neoscopelus macrolepidotus (27); Meso-Bentho
Neoscopelus microchir (25); Meso-Bentho
Salps (25); Meso
Cyclothone sp. (16); Meso-Bathy
Idiacanthus fasciola (16); Meso-Bathy
Sergestidae sp. (16); Meso
Natantia sp. (14); Meso
Diaphus suborbitalis (10); Meso
Gonostoma elongatum (9); Meso-Bathy
Enoploteuthidae sp. (8); Meso-Bathy
Lampanyctus alatus (8); Meso
Oplophoridae sp. (8); Meso-Bathy
Gonostoma atlanticum (7); Meso-Bathy
Euphausiacea sp. (6); Meso
Phyllosoma larvae (6)
Abraliopsis sp. (5); Meso-Bathy
Pasiphaea sp. (5); Meso-Bathy
Sepiolidae sp. (4)
Phronima sp. (3)
Vinciguerria nimbaria (3); Meso
Enoploteuthidae sp. (1); Meso-Bathy
Hygophum hygomii (1); Meso
Day Deep Vicinity
Argyropelecus aculeatus (56); Meso
Pyrosoma sp. (41); Meso
Argyropelecus hemigymnus (36); Meso
Cyclothone sp. (33); Meso-Bathy
Salps (23); Meso
Chauliodus sloani (22); Meso
Diaphus perspicillatus (17); Meso
Oplophoridae sp. (15); Meso-Bathy
Gonostoma atlanticum (14); Meso-Bathy
Diaphus mollis (13); Meso
Phyllosoma larvae (12)
Diaphus dilademalus (11); Meso
Decapterus macarellus (10); Meso
Hygophum hygomii (9); Meso
Loblanchia gemellarii (8); Meso
Medusae (7)
Leptocephali (6); Epi
Paralepididae (larvae/juv) (5); Epi-Bathy
Vinciguerria nimbaria (5); Meso
Cystisoma sp. (4);
Diaphus suborbitalis (4); Meso
Enoploteuthidae sp. (4); Meso-Bathy
Euphausiacea sp. (3)
Cranchiidae sp. (larvae/juv) (2); Meso
Abraliopsis sp. (1); Meso-Bathy
Argyropelecus affinis (1); Meso
Night Shallow Vicinity
Pyrosoma sp. (1829); Meso
Abraliopsis sp. (680); Meso-Bathy
Ceratoscopelus warmingii (127); Meso
Diaphus perspicillatus (101); Meso
Hygophum hygomii (62); Meso
Phyllosoma larvae (44)
Sergestidae sp. (47); Meso
Acanthuridae sp. (larvae/juv) (33); Epi
Gonostoma elongatum (28); Meso-Bathy
Myctophidae sp. (28); Meso
Leptocephali (19); Epi
Lampanyctus alatus (16); Meso
Chauliodus sloani (13); Meso
Astronesthes sp. (12); Meso
Euphausiacea sp. (12); Meso
Notoscopelus resplendens (10); Meso-Bathy
Salps (10); Meso
Benthosema suborbitale (9); Meso
Diaphus sp. (8); Meso
Enoploteuthidae sp. (6); Meso-Bathy
Idiacanthus fasciola (6); Meso-Bathy
Lampanyctus sp. (6); Meso
Nemichthyidae sp. (5); Meso-Bathy
Oplophoridae sp. (5); Meso-Bathy
Cranchia scabra (3); Meso
Night Deep Vicinity
Pyrosoma sp. (299); Meso
Salps (225); Meso
Caridea sp. (122); Meso
Sergestidae sp. (80); Meso
Abraliopsis sp. (60); Meso-Bathy
Ceratoscopelus warmingii (53); Meso
Argyropelecus aculeatus (35); Meso
Gonostoma elongatum (23); Meso-Bathy
Argyropelecus hemigymnus (22); Meso
Hygophum hygomii (22); Meso
Oplophoridae sp. (18); Meso-Bathy
Medusae (16)
Diaphus richardsoni (15); Meso
Diaphus perspicillatus (14); Meso
Lampanyctus alatus (10); Meso
Enoploteuthidae sp. (9); Meso-Bathy
Phyllosoma larvae (8)
Eustomias sp. (7); Meso-Bathy
Pasiphaea sp. (7); Meso-Bathy
Bolinichthys photothorax (6); Meso
Leptocephali (6); Epi
Chauliodus sloani (5); Meso
Neognathophausia ingens (4); Meso
Cyclothone sp. (3); Meso-Bathy
Onychoteuthidae sp. (3); Epi-Meso
Night Intermediate Vicinity
Pyrosoma sp. (93); Meso
Argyropelecus aculeatus (57); Meso
Gonostoma elongatum (28); Meso-Bathy
Ceratoscopelus warmingii (26); Meso
Lampanyctus alatus (19); Meso
Oplophoridae sp. (18); Meso-Bathy
Abraliopsis sp. (17); Meso-Bathy
Sergestidae sp. (12); Meso
Caridea sp. (11); Meso
Salps (11); Meso
Diaphus mollis (10); Meso
Enoploteuthidae sp. (9); Meso-Bathy
Leptocephali (7); Epi
Lobianchia gemellarii (6); Meso
Diaphus dilademalus (5); Meso
Idiacanthus fasciola (5); Meso-Bathy
Cranchiidae sp. (larvae) (4); Meso
Diaphus brachycephalus (4); Meso
Diaphus perspicillatus (4); Meso
Phronima sp. (3)
Funchalia sp. (2); Meso-Bathy
Phyllosoma larvae (2)
Euphausiacea sp. (2)
Histioteuthis sp. (1); Meso
Night SSL
Summit and Flank-associated; resident species
DSL
Depth (m)
Time (hh:mm)
18:07
18:50
19:34
20:17
Day SSL
Summit-associated species
DSL and Flank-associated species
03:10
04:33
Day SSL Vicinity
Intensification of SSL at sunset Vicinity
NightSSL Vicinity
Mid-water migrants/ Non-migrants
Intensification of DSL and Upward Migration at sunset
Mid-water migrants Non-migrants
Delayed migration
11:04
11:46
13:07
13:48
14:30
15:51
16:50
17:39
Sv (dB re 1 m-1)

Figure 9

RGB Composites of MAD-Ridge seamount

Red: 38 kHz; Green: 70 kHz; Blue: 120 kHz

a) Trawl #14

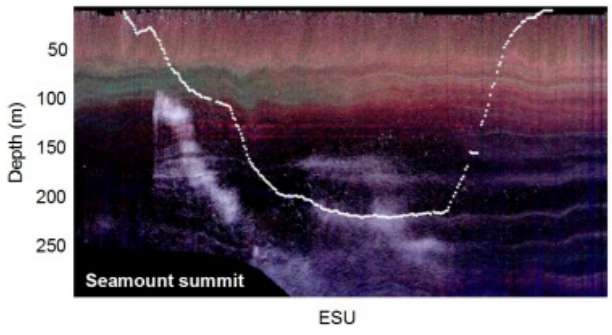

b) Trawl #15

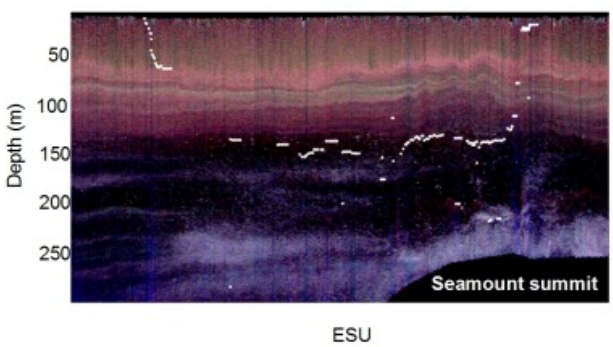

c) Trawl #16

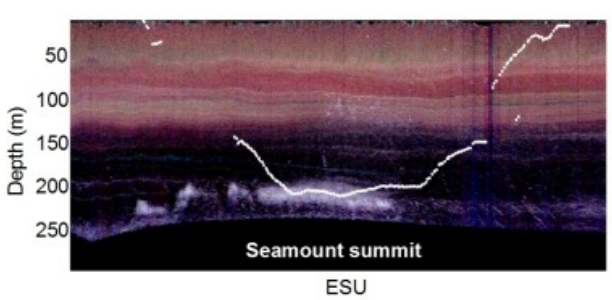

d) Trawl #21

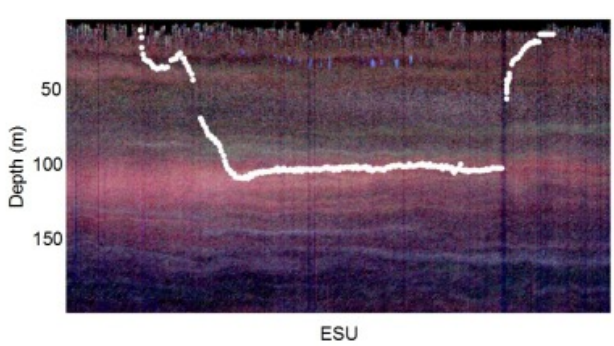

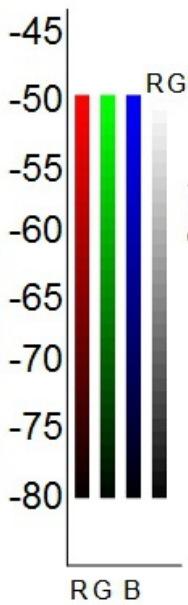

Frequency Diagrams and Frequency Responses

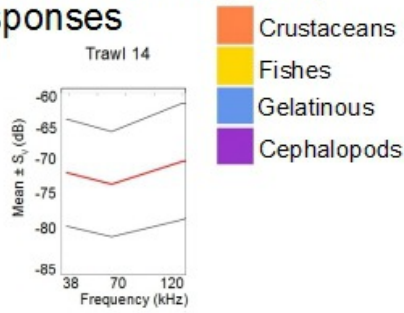

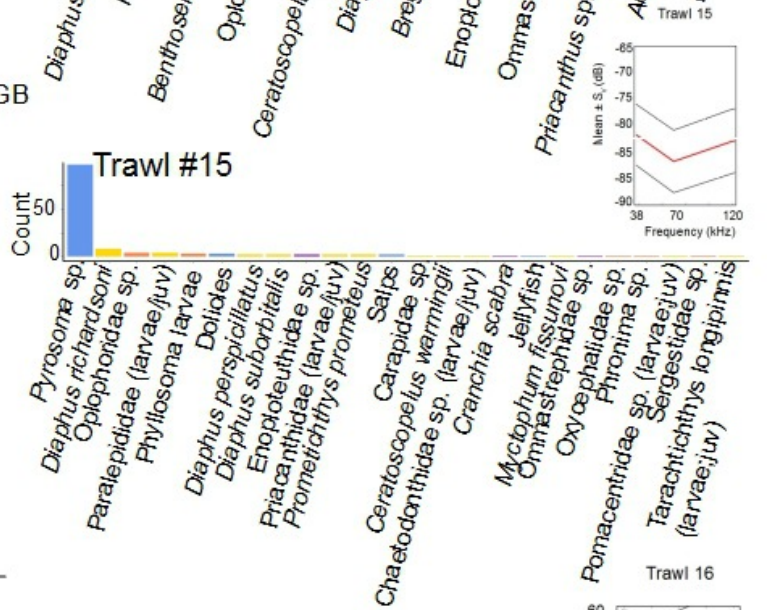

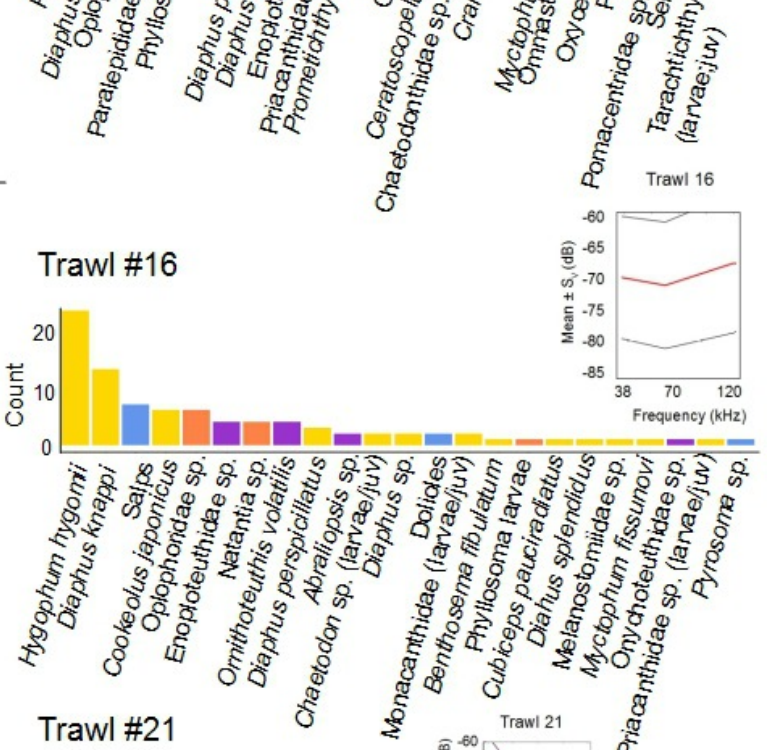

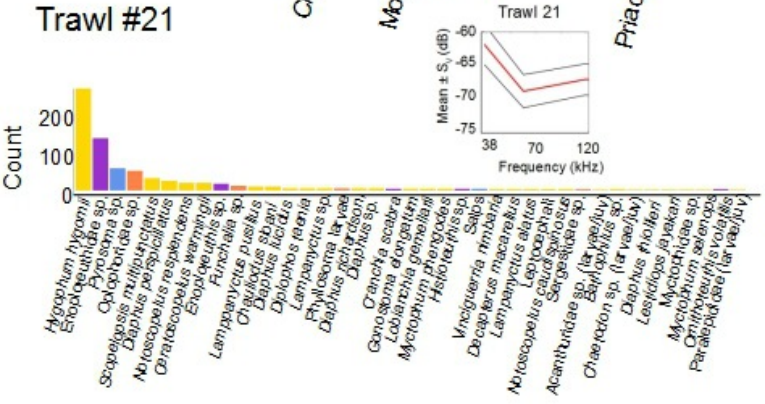

Figure 10

Table 1 Summary of trawl stations at La Pérouse and MAD-Ridge seamounts

Cruise	Trawl #	Latitude Beginning (°)	Longitude Beginning (°)	Maximum Trawl Depth (m)	Trawl Position	Day/Night	Trawling Speed (knots)	Filtered water volume (in 1000 m^3)
La Pérouse	1	-19.77	54.09	590	Vicinity	Night	3.0	837
	2	-19.79	54.10	400	Flank	Night	3.2	379
	3	-19.65	53.85	90	Vicinity	Night	2.7	444
	4	-19.68	54.15	110	Flank	Night	3.0	512
	5	-19.76	54.18	35	Summit	Day	3.6	808
	6	-19.72	54.18	60	Flank	Night	3.0	485
	7	-19.63	54.10	500	Vicinity	Night	3.0	502
	8	-19.80	54.17	430	Vicinity	Night	3.2	512
	9	-19.81	54.08	240	Vicinity	Night	3.2	622
	10	-19.76	54.21	250	Vicinity	Night	4.0	871
MAD-Ridge	1	-27.41	45.67	500	Vicinity (North West)	Day	3.2	228
	2	-27.65	46.43	542	Vicinity (North West)	Night	2.3	211
	3	-27.44	46.23	43	Vicinity (North West)	Night	2.2	163
	4	-27.67	46.44	100	Flank (West)	Day	2.8	249
	5	-27.75	46.28	324	Vicinity (South West)	Night	2.8	270
	6	-27.69	46.46	45	Flank (South West)	Night	2.6	154
	7	-27.64	46.37	437	Vicinity (South West)	Day	3.1	276
	8	-27.78	46.35	38	Flank (South)	Night	2.7	240
	9	-27.70	46.45	76	Vicinity (South East)	Night	2.6	179
	10	-27.60	46.53	470	Flank (North East)	Day	2.2	212
	11	-27.69	46.53	90	Flank (North East)	Night	2.3	172
	12	-27.41	46.38	550	Vicinity (North)	Night	2.8	270
	13	-27.65	46.31	460	Flank (North)	Day	3.2	303
	14	-27.68	46.27	210	Flank (West)	Night	2.7	228
	15	-27.67	46.22	150	Flank (West)	Night	2.1	187
	16	-27.59	46.32	205	Summit	Night	3.4	312
	17	-27.51	46.32	550	Vicinity (North West)	Day	2.3	222